Cortically coordinated NREM thalamocortical oscillations play an essential, instructive role in visual system plasticity

Jaclyn Durkin[a,1], Aneesha K. Suresh[b,1], Julie Colbath[c], Christopher Broussard[d], Jiaxing Wu[e], Michal Zochowski[f,g], and Sara J. Aton[c,2]

[a]Neuroscience Graduate Program, University of Michigan, Ann Arbor, MI 48109; [b]Committee on Computational Neuroscience, University of Chicago, Chicago, IL 60637; [c]Department of Molecular, Cellular, and Developmental Biology, University of Michigan, Ann Arbor, MI 48109; [d]Information Technology Advocacy and Research Support, College of Literature, Science, and the Arts, University of Michigan, Ann Arbor, MI 48109; [e]Program in Applied Physics, University of Michigan, Ann Arbor, MI 48109; [f]Program in Biophysics, University of Michigan, Ann Arbor, MI 48109; and [g]Department of Physics, University of Michigan, Ann Arbor, MI 48109

Edited by Gina G. Turrigiano, Brandeis University, Waltham, MA, and approved August 22, 2017 (received for review June 12, 2017)

Two long-standing questions in neuroscience are how sleep promotes brain plasticity and why some forms of plasticity occur preferentially during sleep vs. wake. Establishing causal relationships between specific features of sleep (e.g., network oscillations) and sleep-dependent plasticity has been difficult. Here we demonstrate that presentation of a novel visual stimulus (a single oriented grating) causes immediate, instructive changes in the firing of mouse lateral geniculate nucleus (LGN) neurons, leading to increased firing-rate responses to the presented stimulus orientation (relative to other orientations). However, stimulus presentation alone does not affect primary visual cortex (V1) neurons, which show response changes only after a period of subsequent sleep. During poststimulus nonrapid eye movement (NREM) sleep, LGN neuron overall spike-field coherence (SFC) with V1 delta (0.5–4 Hz) and spindle (7–15 Hz) oscillations increased, with neurons most responsive to the presented stimulus showing greater SFC. To test whether coherent communication between LGN and V1 was essential for cortical plasticity, we first tested the role of layer 6 corticothalamic (CT) V1 neurons in coherent firing within the LGN-V1 network. We found that rhythmic optogenetic activation of CT V1 neurons dramatically induced coherent firing in LGN neurons and, to a lesser extent, in V1 neurons in the other cortical layers. Optogenetic interference with CT feedback to LGN during poststimulus NREM sleep (but not REM or wake) disrupts coherence between LGN and V1 and also blocks sleep-dependent response changes in V1. We conclude that NREM oscillations relay information regarding prior sensory experience between the thalamus and cortex to promote cortical plasticity.

sleep | vision | thalamocortical | plasticity | coherence

Converging behavioral (1), biochemical (2–4), neuroanatomical (5), and electrophysiological (2, 6–8) evidence supports the idea that following novel sensory experiences, sleep can promote cortical plasticity. The sleep-dependent mechanisms driving these changes have remained elusive. Sleep-associated changes in network activity (1, 6, 7, 9, 10), neuromodulator tone (11), transcription (4), translation (4), and protein phosphorylation (2, 3) have all been correlated with cortical plasticity following novel experiences (12). In recent years, neuroscientists have speculated that the high-amplitude, low-frequency thalamocortical oscillations that characterize nonrapid eye movement (NREM) sleep play a critical role in promoting sensory cortical plasticity and learning (12). While it has been hypothesized that such NREM oscillations promote general synaptic "downscaling" (13), converging data suggest that they could instead promote synaptic strengthening (5–7, 9). While rhythmic stimulation of the cortex at frequencies meant to mimic NREM oscillations (1–2 Hz) is sufficient to promote cortical plasticity and learning (9, 10), it is unclear whether naturally occurring oscillations are necessary for sleep-dependent processes. Another critical question is whether NREM oscillations play an instructive role in experience-initiated plasticity—i.e., whether these oscillations relay information about prior experience through thalamocortical circuitry.

Orientation-specific response potentiation (OSRP) in mouse primary visual cortex (V1) (14) is initiated by a novel visual stimulus (a flickering grating of a single orientation) presented over a period of several minutes (7). OSRP is expressed in V1 several hours later, as enhanced neuronal responses to stimuli of the same orientation; critically, sleep deprivation following visual experience prevents OSRP consolidation (7, 8). Recent data suggest that OSRP is mediated by potentiation of lateral geniculate nucleus (LGN) synapses in V1 (15). To clarify the role of thalamocortical and corticothalamic (CT) communication in OSRP consolidation, we first tested how visual experience alone affected neuronal firing and OSRP in both LGN and V1 neurons and then determined how coherent firing between the two areas was affected during subsequent sleep. We also tested the effects of optogenetic manipulations of layer 6 corticothalamic (CT) neurons, aimed at either mimicking or disrupting NREM sleep oscillations, on both neuronal firing patterns and OSRP following visual experience.

Significance

Previous studies have demonstrated a role of state-specific neural activity in plasticity; however, a mechanism for these changes has yet to be elucidated. Here, we demonstrate that sensory response changes occur in thalamic neurons immediately following novel visual experience, but that subsequent nonrapid eye movement (NREM) oscillations are required for subsequent response changes in the primary visual cortex (V1). Consequently, we show that disruption of NREM oscillations specifically blocks sleep-dependent plasticity in V1. We conclude that following a novel sensory experience, neural activity patterns unique to NREM facilitate transfer of information from the visual thalamus to the V1, leading to adaptive response changes in V1 neurons.

Author contributions: J.D. and S.J.A. designed research; J.D., A.K.S., J.C., and S.J.A. performed research; C.B., J.W., and M.Z. contributed new reagents/analytic tools; J.D., A.K.S., J.C., and S.J.A. analyzed data; and J.D. and S.J.A. wrote the paper.

The authors declare no conflict of interest.

This article is a PNAS Direct Submission.

Freely available online through the PNAS open access option.

[1]J.D. and A.K.S. contributed equally to this work.

[2]To whom correspondence should be addressed. Email: saton@umich.edu.

This article contains supporting information online at www.pnas.org/lookup/suppl/doi:10.1073/pnas.1710613114/-/DCSupplemental.

Results

LGN, but Not V1, Neurons Show Immediate Orientation-Specific Response Changes Following Visual Stimulation. Previous studies [by our laboratory (7, 8) and others (14)] have demonstrated that orientation preference in V1 neurons is unchanged immediately after presentation of a single oriented grating stimulus, even for stimulus durations of up to an hour. To test whether LGN neurons are similarly unaffected across stimulus presentation, we generated orientation tuning curves for individual V1 and LGN neurons in anesthetized mice before and after a 30-min grating presentation. Surprisingly, many LGN neurons showed dramatic orientation-specific response changes during this treatment (e.g., the ratio of neuronal firing rate for X° over the neuronal firing rate for the orthogonal, X + 90°). These increases in X°/X + 90° were present across a number of recordings for different presented stimulus orientations (Fig. 1 and *SI Appendix*, Figs. S1 and S2; $n = 147$ neurons from seven experiments), but, consistent with our previous findings (7), were not seen in V1 neurons recorded from the same mice ($n = 32$ neurons). Among many of the recorded LGN neurons, visually evoked firing-rate responses increased significantly across the 30-min grating presentation, a phenomenon that we had not previously seen in V1 (8) (Fig. 2*A*). The amount that individual neuron firing rates changed across stimulus presentation, while heterogeneous, predicted the amount of change in X°/X + 90° after stimulus presentation (Fig. 2*B* and *SI Appendix*, Fig. S6*A*). This rapid response change did not result in an increase in the proportion of LGN neurons selective for the presented stimulus orientation (*SI Appendix*, Figs. S1 and S2); rather, neuronal firing-rate responses to X° selectively increased (e.g., relative to X + 90° and X ± 45°).

To better understand the relationship of these firing-rate changes to OSRP seen in V1 across a period of poststimulus sleep, we simultaneously recorded both LGN and V1 neurons in nonanesthetized animals during and after presentation of a grating at the beginning of the rest phase (CT0). Here again, we found that firing-rate responses increased significantly across stimulus presentation in LGN, but not in V1 (Fig. 2*C*). Firing increases were not seen in LGN neurons recorded from mice presented with a blank screen [not significant (N.S.); Fig. 2*C*]. Firing-rate increases among LGN neurons during stimulus presentation predicted increases in X°/X + 90° measured across the rest period (Fig. 2*D* and *SI Appendix*, Fig. S6*B*). Critically, as we had previously shown for V1 neurons following OSRP induction (8), firing rates in LGN neurons remained elevated during poststimulus NREM sleep (Fig. 2*E*). Taken together, these data suggest that oriented grating presentation leads to (*i*) rapid changes in X°/X + 90° in LGN neurons and (*ii*) long-lasting changes in firing of LGN neurons during subsequent NREM sleep.

LGN Neurons Show Increased Spike-Field Coherence with NREM Thalamocortical Oscillations During OSRP Consolidation. OSRP is expressed in V1 only after several hours of poststimulus sleep; critically, sleep deprivation following visual experience prevents OSRP consolidation (7, 8) (*SI Appendix*, Fig. S3). To assess whether communication between LGN and V1 changes during poststimulus sleep, we continuously recorded LGN and V1 neuronal firing and corresponding local field potential (LFP) activity (*SI Appendix*, Figs. S4 and S5). Recordings spanned a 24-h period of baseline sleep and wake, a 30-min stimulus presentation, and a subsequent 12-h OSRP consolidation window. We then characterized the temporal relationships [in the form of spike-field coherence (SFC)] between LGN neuronal firing and V1 LFP oscillations during OSRP consolidation (Fig. 3). LGN neuron SFC with V1 delta and spindle oscillations increased during NREM in the hours following oriented grating presentation (Fig. 3*B* and *SI Appendix*, Fig. S6*C*).

We also tested whether LGN neurons underwent an increase in coherent firing during NREM per se by assessing the periodicity of firing before and after oriented grating exposure. We found that following stimulus presentation, coherent LGN neuronal firing in the delta frequency band predicted the extent of their OSRP across the poststimulus period (Fig. 3*C* and *SI Appendix*, Fig. S6*D*). These data suggest that, as is true for V1 neurons (7), waking visual experience leads to changes in LGN neuron coherent firing during subsequent NREM sleep. Because OSRP is present only in the LGN immediately following experience, we hypothesized that LGN-V1 coherence during NREM oscillations could promote sleep-dependent OSRP consolidation in V1.

Layer 6 CT Input Is Sufficient to Drive Coherent Firing in the LGN-V1 Network. CT input is necessary for coordinating NREM delta and spindle oscillations within thalamic circuits (16, 17). Thus, CT-mediated coordination might be critical for promoting the observed changes in LGN-V1 coherence during poststimulus NREM sleep. To test the sufficiency of V1 layer 6 (L6) CT input to drive coherent firing in LGN and V1, we recorded LGN and V1 firing patterns in transgenic mice expressing channelrhodopsin 2 (ChR2) in L6 CT neurons (*Ntsr1:ChR2*) (Fig. 4 *A*, *B*, *G*, and *H* and *SI Appendix*, Fig. S7). After recording baseline activity in both areas, we measured changes in firing rhythmicity in response to rhythmic optogenetic activation of V1 L6 CT neurons across a range

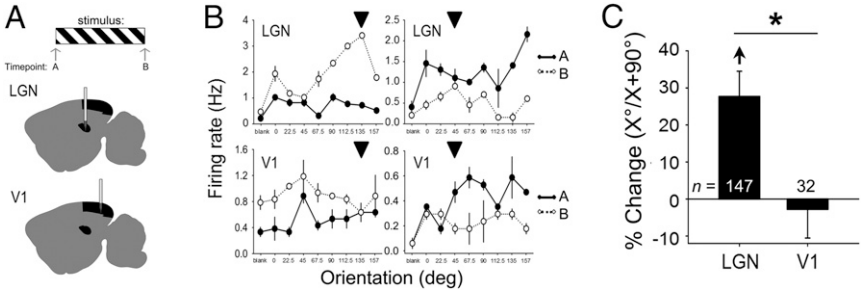

Fig. 1. Visual experience immediately alters response properties in LGN, but not in V1, neurons. (*A*) Visual responses of LGN and V1 neurons were recorded from mice under isoflurane anesthesia. At time point A, mice were presented randomly with a series of oriented full-field grating stimuli (0, 22.5, 45, 67.5, 90, 112.5, 135, and 157.5 degrees) and a blank screen (bl) to assess baseline orientation tuning and visual responsiveness. One stimulus was chosen at random and presented for a 30-min period. At time point B, visual response properties were reassessed. (*B*) Tuning curves for representative LGN neurons (*Top*) show increased relative responses to the presented orientation (vs. other orientations; presented stimulus indicated with arrowhead) from time point A (solid line) to time point B (dotted line). Consistent with our prior findings (7), V1 neurons (*Bottom*) do not show an enhanced response to the presented orientation immediately following stimulus presentation. Values indicate mean firing-rate response (±SEM) to each stimulus. (*C*) Immediately following visual stimulus presentation, LGN neurons (but not V1 neurons) showed a significant increase in relative responsiveness to the presented stimulus orientation [relative to the orthogonal orientation (X°/X + 90°); arrow indicates $P < 0.05$, repeated measures (RM) ANOVA on ranks; *$P < 0.05$ for LGN vs. V1 neurons].

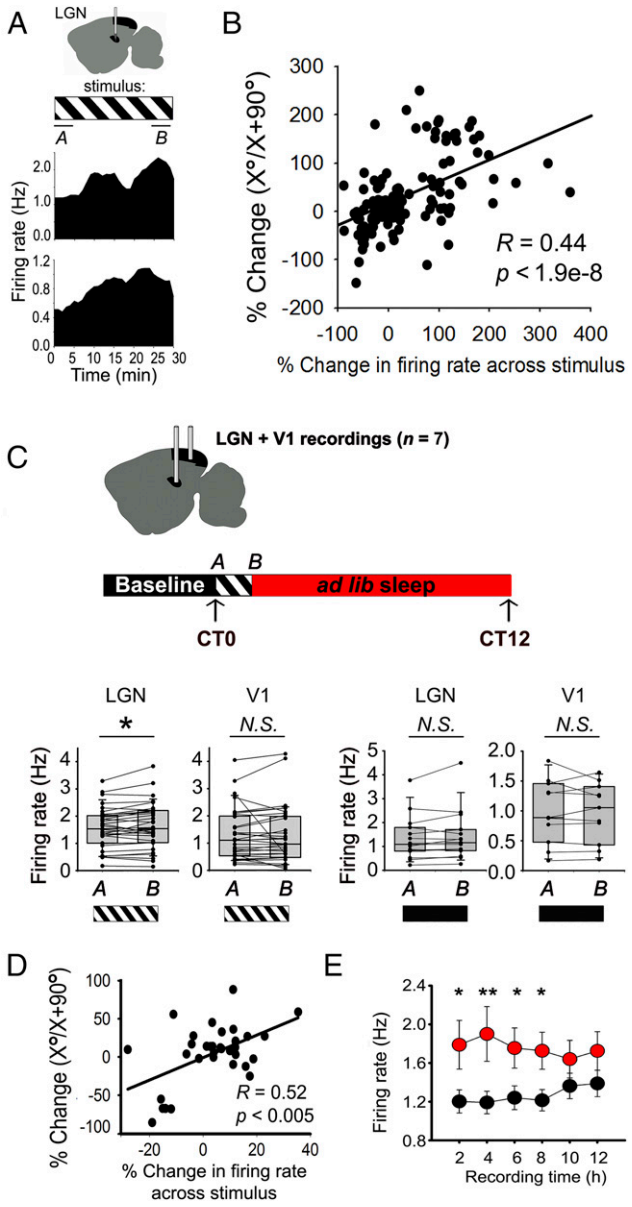

Fig. 2. Stimulus-induced firing enhancement in LGN neurons predicts response changes and persists during subsequent NREM sleep. (*A*) Two representative LGN neurons recorded from an anesthetized mouse show firing-rate increases across the 30-min stimulus presentation (mean rate plotted in 1-min bins). (*B*) Firing-rate increases predicted the change in X°/X + 90° (i.e., OSRP) across stimulus presentation. Pearson product moment *R* and *P* values are shown for 147 LGN neurons. (*C*, *Top*) Mice implanted with electrodes targeting both LGN and V1 were recorded over a 24-h baseline period, presented with an oriented grating at CT0, and then allowed 12 h of ad libitum sleep. Visual response properties were assessed at CT0 and CT12. (*C*, *Bottom Left*) V1 neurons showed no change in firing rate between the first and last 5 min of the 30-min grating presentation (time point A and time point B, respectively, N.S., Wilcoxon signed rank test, $n = 34$ neurons from six mice). However, LGN neuronal firing rates increased significantly ($P = 0.018$, Wilcoxon signed rank test, $n = 35$ neurons). (*C*, *Bottom Right*) Neither V1 nor LGN neurons showed a significant change in firing rate between the first and last 5 min of a 30-min blank screen presentation (N.S., Wilcoxon signed rank test, $n = 16$ and 11 neurons, respectively, from three experiments). (*D*) As was true in anesthetized recordings, firing-rate increases in LGN neurons across stimulus presentation predicted OSRP across the day. Pearson product moment *R* and *P* values are shown for 35 stably recorded LGN neurons. (*E*) Compared with baseline recording (black), LGN neuron firing rates during the first 8 h of poststimulus NREM (red) remained significantly elevated (two-way RM ANOVA, treatment × time interaction $P < 0.001$; $^*P < 0.05$, $^{**}P < 0.01$). N.S., not significant.

of frequencies: 0.5, 1, 2, 3, and 4 Hz. In both V1 and LGN recordings, we observed phase-locking of both neurons' firing and LFP activity to optogenetically induced rhythms of CT activity (Fig. 4 *B* and *H*). Only a subset of stimulation frequencies (1, 2, and 3 Hz) increased V1 neuron firing coherence significantly from baseline (Fig. 4*C*). In contrast, stimulation at all frequencies increased LGN neuron firing coherence and led to more pronounced (i.e., higher amplitude) firing rhythms compared with those induced in V1 (Fig. 4*I*). The proportion of LGN neurons significantly affected by optogenetic stimulation of V1 CT neurons (Fig. 4*L*) was also much greater than the proportion of neurons affected in V1 (Fig. 4*F*).

Optogenetic stimulation of L6 CT neurons similarly affected the rhythmicity of LFP activity in both V1 (Fig. 4 *D* and *E*) and LGN (Fig. 4 *J* and *K*). Optogenetic activation of V1 CT neurons also induced higher-frequency (11–15 Hz) spindle-like LFP events in V1 (*SI Appendix*, Fig. S8*A*). These events were time-locked to rhythmic optogenetic stimulation and varied in density and duration based on stimulation frequency (*SI Appendix*, Fig. S8 *B* and *C*).

Optogenetic Inhibition of L6 CT Neurons Disrupts V1-LGN Coherence During NREM Sleep. We next tested whether optogenetic inhibition of L6 CT neurons could disrupt coherent NREM oscillations following induction of OSRP. To do this, we virally transduced L6 CT neurons in V1 with archaerhodopsin3 (Arch) (18) in L6 CT neurons in V1 (*SI Appendix*, Fig. S9). Light delivery to V1 of transduced mice reliably and reversibly suppressed firing in the majority of V1 L6 neurons (and target neurons in the LGN) over a timescale of seconds to minutes (Fig. 5*A* and *SI Appendix*, Fig. S10). NREM-targeted light delivery in the hours following visual stimulus presentation significantly reduced delta and spindle-frequency LFP power in V1, relative to baseline NREM sleep (Fig. 5*B* and *SI Appendix*, Fig. S11). Spindle-frequency coherence between LGN LFPs and V1 LFPs was significantly reduced during NREM-targeted inhibition of V1 CT neurons (Fig. 5*C*). This was associated with a disruption in the temporal relationship between V1 and LGN fields, leading to longer delays (relative to lag times seen at baseline) between V1 and LGN spindle-frequency activity (an effect not seen in

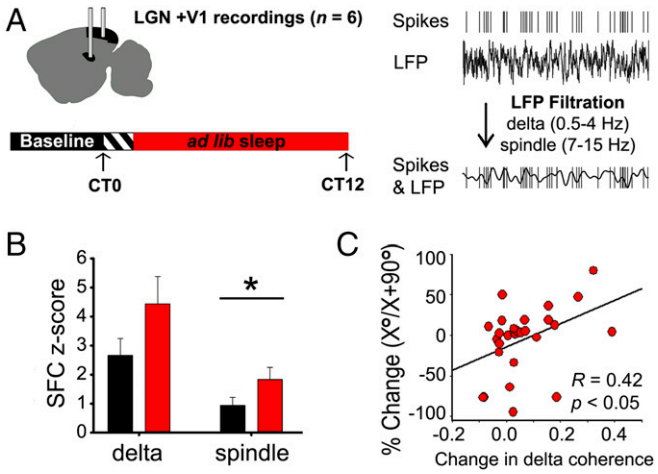

Fig. 3. LGN neurons show increased SFC with V1 NREM oscillations following stimulus presentation. (*A*) Mice implanted with electrodes targeted to LGN and V1 were recorded as described in Fig. 2*C*. LGN SFC with V1 oscillations was calculated during NREM at baseline and after stimulus presentation. (*B*) Following stimulus presentation, LGN neurons showed significantly increased SFC with V1 LFPs filtered at spindle frequency ($^*P = 0.01$, Wilcoxon signed rank test). There was a similar trend for increased SFC in the delta frequency band ($P = 0.088$, Wilcoxon signed rank test). (*C*) Increases in LGN neurons firing periodicity at delta frequencies during NREM predicted their ORSP across the day. Pearson product moment *R* and *P* values are shown for 35 stably recorded LGN neurons.

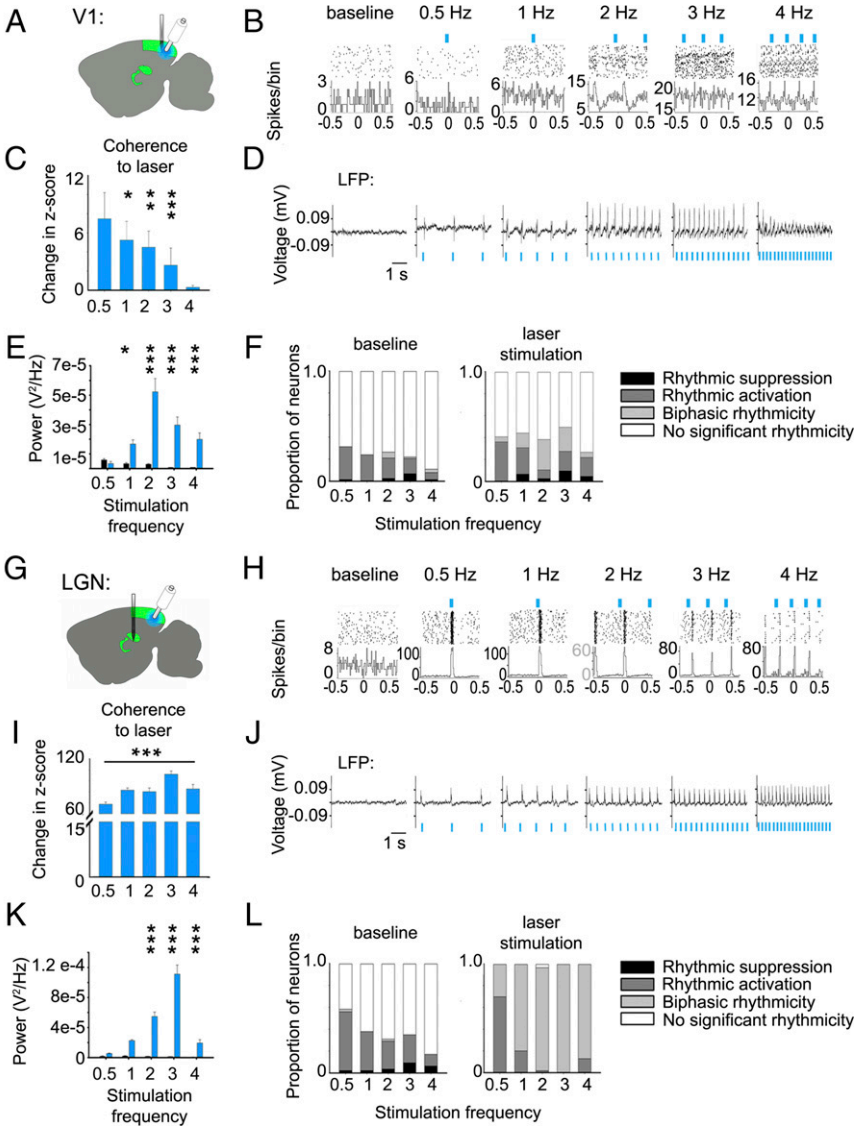

Fig. 4. Stimulation of ChR2-expressing CT neurons induced coherent firing in V1 and LGN. (*A*) For V1 recordings from anesthetized *Ntsr1::ChR2* mice, a 32-channel silicone probe was lowered into the V1 until stable recordings were obtained, and an optical fiber was targeted to V1 L6. Neuronal responses were aggregated across all layers of the visual cortex. (*B*) Peri-event spike rasters and histograms are shown for a representative neuron at baseline and during optogenetic stimulation of V1 L6. (*C*) V1 neurons showed increased coherent firing at the frequency of optogenetic stimulation compared with baseline. $*P < 0.05$, $**P < 0.01$, and $***P < 0.001$, Wilcoxon signed rank test. (*D*) LFP activity is shown at baseline and during optogenetic stimulation. (*E*) LFP power at the frequency of stimulation (blue bars) was significantly increased from baseline (black bars) values during stimulation. $*P < 0.05$ and $***P < 0.001$, Holm–Sidak post hoc test vs. baseline. (*F*) The proportion of V1 neurons that showed statistically significant ($P < 0.01$) periodic suppression and activation are shown for each frequency during baseline (*Left*) and during optogenetic stimulation (*Right*). (*G*) For LGN neuronal recordings in anesthetized *Ntsr1::ChR2* mice, a 32-channel silicone probe was lowered into LGN until stable recordings were obtained, and an optical fiber was targeted to V1 L6. (*H–L*) Data for LGN spiking and LFP activity are shown as in *B–F*. For *L*, all LGN neurons showed significant rhythmicity during optogenetic stimulation of L6 CT neurons.

the absence of CT inhibition; Fig. 5*D*; N.S. for delta frequency activity, *SI Appendix*, Fig. S12). LGN neuron SFC with V1 delta and spindle oscillations was also significantly reduced during V1 CT inhibition (Fig. 5*E*). Taken together, these changes demonstrate that inhibition of L6 CT neurons desynchronizes NREM oscillations and thalamocortical communication during OSRP consolidation.

Optogenetic Inhibition of CT Neurons During NREM, but Not REM or Wake, Disrupts V1 Plasticity. We next tested the necessity of state-specific CT activity for consolidation of OSRP in V1. Following presentation of a visual stimulus to induce OSRP, Arch-expressing mice underwent a 6-h period of state-targeted V1 CT neuron inhibition during bouts of NREM, REM, or wake (Fig. 6*A* and *SI Appendix*, Fig. S15). This intervention had no significant effect on sleep architecture across either the 6-h period of optogenetic inhibition or the 6 h of subsequent recovery sleep (N.S., two-way ANOVA; *SI Appendix*, Figs. S16 and S17). There were no significant differences in V1 OSRP between control mice without CT neuron inhibition, mice with REM- or wake-targeted inhibition of CT neurons, and mice expressing a control (YFP) transgene following NREM-targeted light delivery to V1 (N.S., Holm–Sidak test). However, inhibition of CT neurons during NREM blocked OSRP in a manner similar to sleep deprivation ($P < 0.001$, ANOVA; Fig. 6*B* and *SI Appendix*, Figs. S19 and S20). Similarly, the distribution of orientation preference changed across a period of sleep (leading to a greater proportion of neurons preferring X°) in control mice without CT neuron inhibition, mice with REM- or wake-targeted inhibition of CT

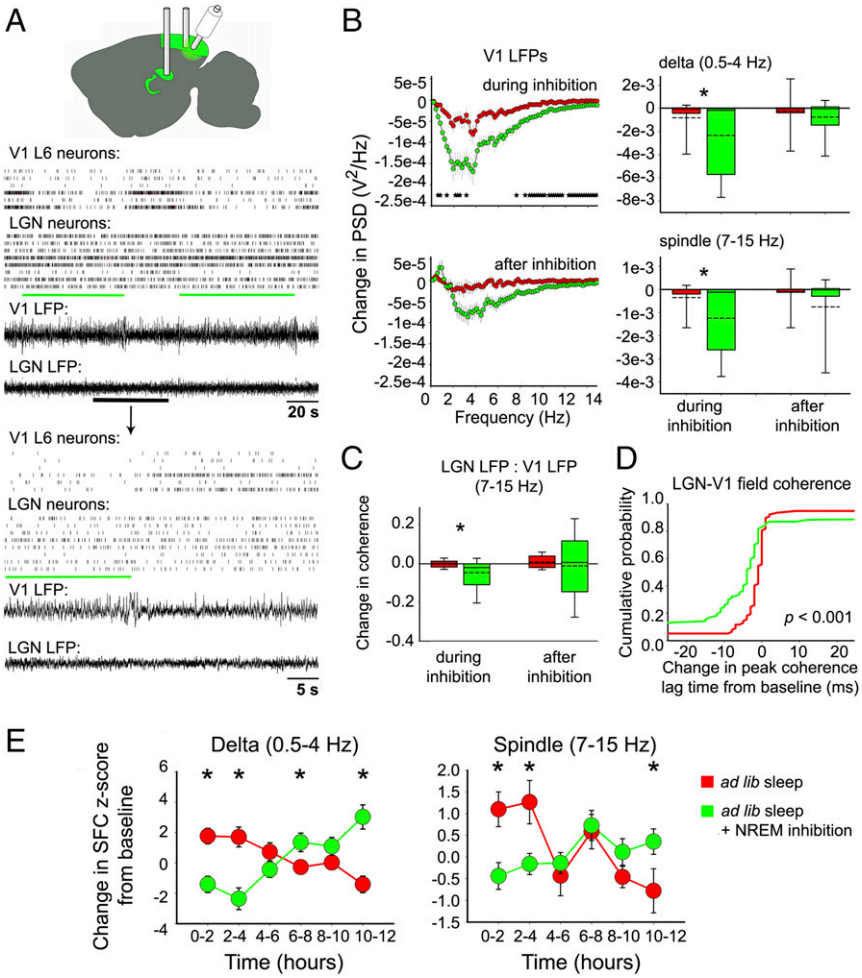

Fig. 5. NREM-targeted optogenetic inhibition of V1 L6 CT neurons disrupts coherent thalamocortical oscillations. (*A*) LGN and V1 activity was simultaneously recorded in *Ntsr1-cre* transgenic mice transduced with Arch-GFP. L6 V1 CT neurons were optogenetically inhibited across bouts of NREM sleep in the first 6 h of the poststimulus ad libitum sleep period. Light delivery reliably inhibited L6 neuronal firing and slightly reduced firing in LGN neurons. (*B*, *Left*) V1 power spectral density during NREM-targeted L6 inhibition (expressed as a change from baseline; $n = 64$ LFPs from 11 mice, green) was significantly reduced relative to that of no-laser (noninhibited) control mice ($n = 76$ LFPs from 14 mice, red; $^*P < 0.05$ for no-laser vs. inhibited conditions, Bonferroni-corrected Student's *t* test for each frequency value). (*B*, *Right*) Total integrated spectral power changes (from baseline) across delta (0.5–4 Hz) and spindle (7–15 Hz) frequency bands significantly decreased during inhibition (green; * indicates $P < 0.01$ and $P < 0.001$, respectively) compared with no-laser control mice (red). Power recovered to normal levels after the 6-h inhibition period (N.S., Mann–Whitney rank sum test). (*C*) Spindle-frequency coherence decreased between V1 and LGN LFPs during NREM inhibition [$n = 77$ LFP pairs recorded across both inhibition and control conditions in four mice; $P < 0.001$ (indicated by *) and $P = 0.786$, respectively, for during and after 6-h NREM-targeted inhibition; Mann–Whitney rank sum test]. (*D*) NREM-targeted inhibition caused an increase in the time lag between V1 and LGN LFPs at their maximum spindle-frequency coherence, relative to baseline ($P < 0.001$, Kolmogorov–Smirnov test for inhibition vs. no-laser conditions). (*E*) NREM-targeted inhibition of L6 CT neurons decreased interareal SFC between LGN and V1. LGN spike to V1 LFP SFC at delta frequency: condition × time interaction $P < 0.001$; at spindle frequency: main effect of time $P = 0.01$ and condition × time interaction $P < 0.001$; two-way RM ANOVA; $n =$ 54 neurons from seven mice and 40 neurons from five mice for no-laser control and inhibition conditions, respectively. V1 spike and LGN LFP SFC at delta frequency: main effect of time $P < 0.05$ and condition × time interaction $P < 0.001$ and at spindle frequency: N.S.; $n = 29$ neurons from six mice and 17 neurons from four mice for no-laser control and inhibition conditions, respectively. $^*P < 0.05$, Holm–Sidak post hoc test.

neurons, and mice expressing a control (YFP) transgene, but not mice with NREM-targeted inhibition (*SI Appendix*, Fig. S20). NREM-targeted CT inhibition appeared to specifically disrupt sleep-associated OSRP consolidation, as there were no immediate effects of L6 CT neuron inhibition on orientation tuning in any layer of V1 (*SI Appendix*, Fig. S14). Thus, these data suggest that CT coordination of NREM oscillations in the LGN-V1 network plays a critical role in promoting sleep-dependent V1 OSRP.

Discussion

Our present data show that novel visual experience rapidly alters response properties in LGN neurons to enhance their responsiveness in favor of the presented stimulus orientation. This change is selective, occurring before expression of V1 OSRP, which relies on subsequent sleep (7) (*SI Appendix*, Fig. S3). This experience also alters the temporal relationship between LGN neuron firing and V1 activity during subsequent NREM oscillations.

Previous studies have found that a subset of mouse LGN neurons shows orientation-selective responses (19–21). However, until now, it was unknown whether orientation-selective responses in the LGN (like that in the V1) can change in response to visual experience. Our data suggest that sensory response plasticity does occur in LGN neurons. Prior work in the somatosensory system (22, 23) suggested that thalamic neurons can change their response properties rapidly following disruption of peripheral sensory input. These data demonstrate that, following novel sensory experience, thalamic neurons in the visual pathway also show rapid response plasticity and that these changes precede response plasticity in V1.

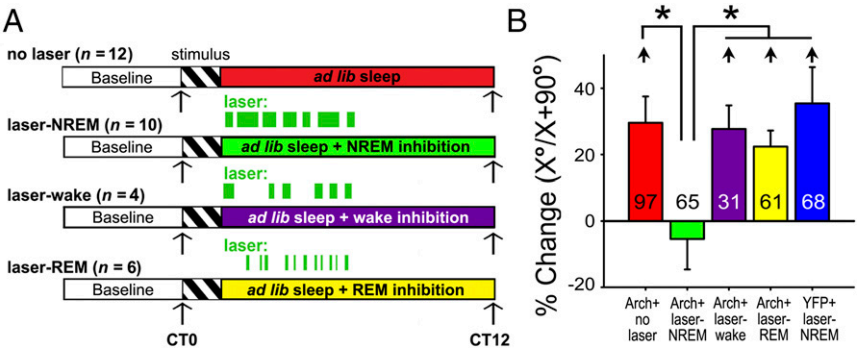

Fig. 6. NREM-targeted inhibition of CT neurons disrupts consolidation of V1 response plasticity after visual experience. (*A*) Experimental paradigm for evaluating the effects of poststimulus-state–targeted optogenetic inhibition of V1 CT neurons on OSRP consolidation. (*B*) NREM-targeted inhibition of V1 CT neurons (laser-NREM) reduced OSRP in V1, while inhibition in other states did not affect OSRP. *$P < 0.001$, Dunn's post hoc test versus no-laser controls, laser-wake, laser-REM, and YFP-expressing control mice with light delivery targeted to V1 during NREM ($P < 0.001$; Kruskal–Wallis ANOVA on ranks). With the exception of neurons recorded from mice with NREM-targeted inhibition, neurons recorded from all groups showed a significant increase in relative responsiveness to the presented stimulus orientation [relative to the orthogonal orientation (X°/X + 90°); short arrows indicate $P < 0.05$, RM ANOVA on ranks].

Why does subsequent OSRP in V1 require poststimulus sleep? One possibility is that information is relayed between LGN and V1 during poststimulus NREM, which in turn drives plasticity in the cortex. This interpretation is consistent with what is known about the circuit-level mechanisms of OSRP consolidation. LGN-to-V1 long-term potentiation (LTP) and OSRP are mutually occluding in vivo (15), suggesting that potentiation of thalamocortical synapses underlies OSRP consolidation in V1. We have previously shown that OSRP consolidation is dependent on poststimulus sleep (7, 8). Here we show that in freely sleeping mice, disruption of V1 CT neuron activity during NREM oscillations is sufficient to block OSRP consolidation. While CT neurons also influence the firing of neurons in the other layers of V1 (24), we find that their effects on firing among LGN neurons are much more widespread and dramatic (Fig. 4). We also find that optogenetic inhibition of CT neurons disrupts communication between LGN and V1 during NREM delta and spindle oscillations (Fig. 5). Because we have previously shown that coherent firing of V1 neurons during NREM oscillations predicts the extent of OSRP consolidation (7), a parsimonious interpretation is that thalamocortical coherence during NREM is essential for promoting OSRP in V1. Based on our current data, we conclude that information regarding stimulus characteristics of prior experience is relayed between the thalamus and cortex during subsequent NREM oscillations.

We find that V1-to-LGN CT communication, which coordinates thalamocortical oscillations associated with NREM sleep, plays an essential role for consolidating sensory response plasticity in V1.

Materials and Methods

All animal procedures were approved by the University of Michigan Institutional Animal Care and Use Committee. For anesthetized recording of visual response properties, or effects of L6 stimulation, 2- to 3-mo-old mice were anesthetized with isoflurane, and a 32-site silicon probe was inserted into either V1 or LGN for neuronal recording. For chronic recording from behaving mice, 2-mo-old mice were implanted with drivable headstages composed of two bundles with seven stereotrodes each, using previously described methods (7). Signals from each electrode were split and differentially filtered to obtain spike data and LFP data at each recording site. Individual neurons were tracked throughout the experiment as described previously (7, 25). Complete materials and methods are in *SI Appendix, SI Materials and Methods*.

ACKNOWLEDGMENTS. We thank Sha Jiang and Amanda Morrison for expert technical assistance with these studies. Support for this research was provided by a Young Investigator Award from the Brain and Behavioral Research Foundation; an Alfred P. Sloan Foundation Fellowship; research Grant EY021503 from the National Institutes of Health (to S.J.A.); and a National Science Foundation Graduate Research Fellowship (to J.D.).

1. Huber R, Ghilardi MF, Massimini M, Tononi G (2004) Local sleep and learning. *Nature* 430:78–81.
2. Aton SJ, et al. (2009) Mechanisms of sleep-dependent consolidation of cortical plasticity. *Neuron* 61:454–466.
3. Dumoulin MC, et al. (2015) Extracellular signal-regulated kinase (ERK) activity during sleep consolidates cortical plasticity in vivo. *Cereb Cortex* 25:507–515.
4. Seibt J, et al. (2012) Protein synthesis during sleep consolidates cortical plasticity in vivo. *Curr Biol* 22:676–682.
5. Yang G, et al. (2014) Sleep promotes branch-specific formation of dendritic spines after learning. *Science* 344:1173–1178.
6. Aton SJ, et al. (2013) Visual experience and subsequent sleep induce sequential plastic changes in putative inhibitory and excitatory cortical neurons. *Proc Natl Acad Sci USA* 110:3101–3106.
7. Aton SJ, Suresh A, Broussard C, Frank MG (2014) Sleep promotes cortical response potentiation following visual experience. *Sleep* 37:1163–1170.
8. Durkin J, Aton SJ (2016) Sleep-dependent potentiation in the visual system is at odds with the synaptic homeostasis hypothesis. *Sleep* 39:155–159.
9. Chauvette S, Seigneur J, Timofeev I (2012) Sleep oscillations in the thalamocortical system induce long-term neuronal plasticity. *Neuron* 75:1105–1113.
10. Miyamoto D, et al. (2016) Top-down cortical input during NREM sleep consolidates perceptual memory. *Science* 352:1315–1318.
11. Gais S, Born J (2004) Low acetylcholine during slow-wave sleep is critical for declarative memory consolidation. *Proc Natl Acad Sci USA* 101:2140–2144.
12. Aton SJ (2013) Set and setting: How behavioral state regulates sensory function and plasticity. *Neurobiol Learn Mem* 106:1–10.
13. Tononi G, Cirelli C (2003) Sleep and synaptic homeostasis: A hypothesis. *Brain Res Bull* 62:143–150.
14. Frenkel MY, et al. (2006) Instructive effect of visual experience in mouse visual cortex. *Neuron* 51:339–349.
15. Cooke SF, Bear MF (2010) Visual experience induces long-term potentiation in the primary visual cortex. *J Neurosci* 30:16304–16313.
16. Contreras D, Destexhe A, Sejnowski TJ, Steriade M (1996) Control of spatiotemporal coherence of a thalamic oscillation by corticothalamic feedback. *Science* 274:771–774.
17. Timofeev I, Steriade M (1996) Low-frequency rhythms in the thalamus of intact-cortex and decorticated cats. *J Neurophysiol* 76:4152–4168.
18. Chow BY, et al. (2010) High-performance genetically targetable optical neural silencing by light-driven proton pumps. *Nature* 463:98–102.
19. Piscopo DM, El-Danaf RN, Huberman AD, Niell CM (2013) Diverse visual features encoded in mouse lateral geniculate nucleus. *J Neurosci* 33:4642–4656.
20. Zhao X, Chen H, Liu X, Cang J (2013) Orientation-selective responses in the mouse lateral geniculate nucleus. *J Neurosci* 33:12751–12763.
21. Tang J, Ardila Jimenez SC, Chakraborty S, Schultz SR (2016) Visual receptive field properties of neurons in the mouse lateral geniculate nucleus. *PLoS One* 11:e0146017.
22. Nicolelis MA, Lin RC, Woodward DJ, Chapin JK (1993) Induction of immediate spatiotemporal changes in thalamic networks by peripheral block of ascending cutaneous information. *Nature* 361:533–536.
23. Krupa DJ, Ghazanfar AA, Nicolelis MA (1999) Immediate thalamic sensory plasticity depends on corticothalamic feedback. *Proc Natl Acad Sci USA* 96:8200–8205.
24. Bortone DS, Olsen SR, Scanziani M (2014) Translaminar inhibitory cells recruited by layer 6 corticothalamic neurons suppress visual cortex. *Neuron* 82:474–485.
25. Ognjanovski N, et al. (2017) Parvalbumin-expressing interneurons coordinate hippocampal network dynamics required for memory consolidation. *Nat Commun* 8:15039.

SI Appendix

Cortically-coordinated NREM thalamocortical oscillations play an essential, instructive role in visual system plasticity.

Jaclyn Durkin[2*], Aneesha K. Suresh[1*], Julie Colbath[3], Christopher Broussard[4], Jiaxing Wu[5], Michal Zochowski[6,7], Sara J. Aton[3#]

[1] Committee on Computational Neuroscience, University of Chicago, Chicago, IL, 60637

[2] Neuroscience Graduate Program, University of Michigan, Ann Arbor, MI, 48109

[3] Department of Molecular, Cellular, and Developmental Biology, University of Michigan, Ann Arbor, MI, 48109

[4] College of Literature, Science, and the Arts Information Technology Advocacy and Research Support, University of Michigan, Ann Arbor, MI, 48109

[5] Program in Applied Physics, University of Michigan, Ann Arbor, MI, 48109

[6] Program in Biophysics, University of Michigan, Ann Arbor, MI, 48109

[7] Department of Physics, University of Michigan, Ann Arbor, MI, 48109

* these two authors contributed equally to the manuscript

[#] Correspondence should be addressed to:
Sara J. Aton
University of Michigan
Department of Molecular, Cellular, and Developmental Biology
830 N. University Ave.
3126 Kraus Natural Science Building
Ann Arbor, MI 48109, USA
email: saton@umich.edu

SI Materials and Methods:

Mouse husbandry

All animal husbandry and surgical/experimental procedures were approved by the University of Michigan IACUC. Following surgical procedures, mice were individually housed in standard caging with beneficial environmental enrichment (nesting material, toys, and novel foods) throughout all subsequent experiments. With the exception of OSRP experimental days, during which lights were kept off, lights were maintained on a 12 h:12 h light: dark cycle (lights on at 8 AM), and food and water were provided *ad lib*.

Anesthetized recordings of visual response properties

For anesthetized recording of visual responses from LGN and V1 **(Figs. 1 & 2A-B)**, C57BL/6J mice were anesthetized with isoflurane (0.5-0.8%) and 1 mg/kg chlorprothixene (Sigma). A 2-shank, linear silicon probe (250 μm spacing between shanks) with 25 μm spacing between recording sites (16 sites/shank; Cambridge Neurotech) was slowly advanced into LGN or V1 until stable recordings (with consistent spike waveforms continuously present for at least 30 min prior to baseline recording) were obtained. At each recording site, following a baseline recording, anesthetized mice were presented with phase-reversing grating stimuli (spatial frequency 0.05 cycles/degree, 100% contrast, reversal frequency 1.0 Hz) of 8 orientations (0, 22.5, 45, 67.5, 90, 112.5, 135, or 157.5 degrees from horizontal) and a blank screen (to assess spontaneous firing) in the visual field contralateral to the recorded hemisphere. Stimuli were presented in an interleaved manner, to assess baseline visual properties. Mice were then presented a single oriented grating, chosen at random, over a period of 30

min. Immediately following stimulus presentation, mice were again presented with a series of 8 gratings and blank screen to reassess visual response properties. OSRP and changes in other neuronal visual response properties were quantified as described below. Following all recordings, mice were euthanized and perfused for verification of microelectrode placement.

Optogenetic stimulation of L6 CT neurons

For experiments described in **Figs. 4 & S8,** *Ntsr1-Cre* mice (which express Cre recombinase selectively in L6 corticothalamic neurons (1); B6.FVB(Cg)-Tg(Ntsr1-cre)GN220Gsat/Mmucd; Jackson) were crossed to B6;129S-*Gt(ROSA)26Sor*$^{tm32(CAG-COP4*H134R/EYFP)Hze}$/J mice (Jackson laboratories) to yield mice expressing Channelrhodopsin-2 (ChR2) specifically in L6 CT neurons (*Ntsr1::Chr2*). To assess the effects of CT stimulation on LGN and V1 neurons, *Ntsr1::Chr2* mice were anesthetized with isoflurane and chlorprothixene as described above. A 32-site silicon probe with 250 μm spacing (Cambridge Neurotech) was slowly advanced into right hemisphere LGN or V1 until stable recordings were obtained. And optical fiber was placed 0.5 mm below the cortical surface for delivery of laser light to V1 L6 neurons. A 15-min baseline was recorded, followed by 5-min periods of rhythmic optogenetic stimulation with 473 nm laser light (approximately 3 mW/mm^2; CrystaLaser) at the following frequencies: 0.5, 1, 2, 3, and 4 Hz. Stimulation periods were separated by 10-min intervals to allow neuronal firing to return to baseline levels. Following all optogenetic experiments, mice were perfused and brains were processed for histological assessment. Optic fiber and electrode position were validated prior to data analysis.

Surgical procedures

For chronic recordings in **Figs. 2 & 3,** 2 month old male and female C57BL/6J mice were implanted with custom-built drivable headstages (EIB-36 Neuralynx) under isoflurane anesthesia, using previously described techniques (2). Each headstage was composed of two bundles (each approximately 200 μm in diameter) of seven stereotrodes each (25 μm nichrome wire, California Fine Wire; Grover Beach, CA). For combined V1/LGN recording (**Figs. 2 & 3**), one bundle was placed in right hemisphere LGN (2.25 mm posterior and 2.25 mm lateral from bregma, 2.25 mm ventral to cortical surface) and the other in ipsilateral V1 (3.0 mm posterior and 2.5 mm lateral from bregma, 0.2-0.5 mm ventral to cortical surface). Reference and ground electrodes were placed over left hemisphere V1 and cerebellum, respectively, and three electromyography (EMG) electrodes were placed deep in the nuchal muscle.

For optogenetic inhibition of L6 V1 neurons (**Fig. 5 & 6**), 6 week old, male and female *Ntsr1-cre* transgenic mice underwent bilateral V1 transduction with AAV9.CBA.Flex.Arch-GFP.WPRE.SV40 ("Arch-GFP"; Addgene 22222; PENN Vector core). A volume of 1 µl was injected via a 33 gauge beveled syringe needle at a rate of 0.2 µl/min (3.0 mm posterior and 2.5 mm lateral from bregma, 0.5-0.7 mm ventral to cortical surface). A second group of *Ntsr1-cre* mice were transduced with a YFP (control) expression vector AAV9.EF1a.DIO.eYFP.WPRE.hGH (Addgene 27056; PENN Vector core). Viral titers were between 1.61e13 and 4.65e13 GC/ml. Mice were allowed to recover for 2-3 weeks before implantation with drivable headstages. For combined

V1/LGN recording (**Fig. 5**), one bundle was placed in right hemisphere LGN (2.25 mm posterior and 2.25 mm lateral from bregma, 2.25 mm ventral to cortical surface) and the other in ipsilateral V1 (3.0 mm posterior and 2.5 mm lateral from bregma, 0.2-0.5 mm ventral to cortical surface). An optical fiber was placed adjacent to V1 electrodes. For V1-only recordings (**Fig. 6**), the two bundles were placed into right hemisphere V1, 1.0 mm apart, with the optical fiber tip equidistant between them. Reference, ground, and EMG electrodes were placed as described above.

Chronic stereotrode recording

After mice recovered from surgical procedures (1-2 weeks), chronic stereotrode recording was carried out using previously-described procedures (2, 3). Mice (in their home cage) were placed inside a sound-attenuated recording chamber (Med Associates) and were tethered using a lightweight cable for neural recording. Mice were habituated to daily handling, restraint, and head fixation over a period of 5 days. During this period, electrode bundles were lowered into V1 and/or LGN in 10-20 μm steps until stable neuronal recordings were obtained. Recording stability was defined by the continuous presence of spike waveforms on individual electrodes for at least 24 h prior to the onset of baseline recording. Signals from each electrode were split and differentially filtered to obtain spike data (200 Hz-8 kHz) and LFP/EMG activity (0.5-200 Hz). Data were amplified at 20 ×, digitized, further digitally amplified at 20-100 ×, and recorded using Plexon Omniplex software and hardware (Plexon Inc.; Dallas, TX). For all chronic recordings, single-unit data was referenced locally (e.g., intra-LGN for LGN

recordings; intra-V1 for V1 recordings) to a recording channel without single-unit activity, to eliminate low-frequency noise.

OSRP induction and measurement

A continuous 24-h baseline recording was carried out for each mouse, starting at CT0. The following day at CT0, mice were head-fixed. Phase-reversing gratings (spatial frequency 0.05 cycles/degree, 100% contrast, reversal frequency 1.0 Hz) of 4 orientations (0, 45, 90, and 135 degrees from horizontal) and a blank screen (for assessment of spontaneous activity) were presented to the left visual field (i.e., contralateral to the hemisphere in which visual responses were recorded. Each of these stimuli was presented 8 times (10 s/presentation) in a random, interleaved fashion. Neuronal firing rate responses were quantified and averaged for each stimulus orientation (and blank screen). Immediately following this baseline test, a single grating stimulus (of a randomly-selected orientation) was continuously presented over a 30-min period to induce OSRP. Firing rate changes in LGN and V1 neurons across stimulus presentation were calculated by measuring each neuron's average firing rates over the first and last 5 min of stimulus presentation.

Mice were then returned to their home cage and recordings continued until CT12 in complete darkness (to prevent additional visual experience). Between 30-min grating presentation and testing, mice were either allowed *ad lib* sleep, or were kept awake over the first 6 h, using gentle handling (2). For state-specific optogenetic inhibition (**Figs. 5 & 6**), freely-sleeping mice had green laser light (532 nm; 1-10 mW/mm^2)

delivered to V1 over the first 6 h, during bouts of either NREM (laser-NREM; *n* = 10 experiments with Arch-GFP-expressing mice, *n* = 8 experiments with YFP-expressing mice), REM (laser-REM; *n* = 6), or wake (laser-wake; *n* = 4) (with behavioral state assessed in real-time, based on LFP activity, EMG activity, and infrared video recording of animal behavior). A group of *n* = 12 Arch-GFP-expressing mice underwent no optogenetic manipulation (no laser control mice) but were otherwise treated identically. *Post hoc* analysis of laser targeting efficiency was calculated as the percent of light delivery that was properly targeted to the state, and the percent of the state that received light coverage (**Fig. S16**).

At CT12, mice were again head-fixed and presented with a series of gratings to re-assess orientation preference. Orientation preference for stably-recorded neurons (i.e., those with consistent spike waveforms on the two stereotrode channels across 24-h baseline recording, and across the 12-h OSRP experiment) was quantified as the ratio of mean firing rate responses for the presented orientation (X°) to that of the orthogonal to presented stimulus (X+90°) as described previously. Changes in this measure were quantified by subtracting CT0 baseline (X°/X+90°) ratio from CT12 evening (X°/X+90°) ratio; this difference was then expressed as a percent change from baseline (**Fig. 1C**, **Fig. 6B**, **Fig. S1B, and Fig. S3B**). As an additional measure, changes in the ratio of responsiveness to the presented orientation and to oblique (±45°) orientations (X°/X±45°) were calculated (**Fig. S1**, **& Fig S18B**). An orientation selectivity index (OSI90; used to indicate the strength or orientation tuning, regardless or orientation preference; **Fig. S1E & Fig. S18C**) was also calculated for each neuron, as 1 -

[(average firing rate at 90 degrees from preferred orientation)/(average firing rate at the preferred stimulus orientation)](4)*.* Neuronal visual responsiveness (to any visual stimulus) was assessed statistically using previously-described ANOVA-based methods (5); only visually responsive neurons were included in analysis of OSRP. Using this metric, the proportion of V1 neurons classified as visually responsive vs. non-responsive (**Fig. S20B**) was similar to that reported elsewhere (6). With the exception of data presented in **Figs. S2B & S20B**, only visually responsive neurons were included in analyses of visual response properties and OSRP. There were no significant differences between male and female mice with regards to OSRP expression within control (no laser) conditions (p = 0.70, Mann Whitney rank sum test).

Histology and immunohistochemistry

At the conclusion of each recording, mice were deeply anesthetized with barbiturate injection, and an electrolytic lesion was made at each electrode site (2 mA, 3s per electrode). Mice were then perfused with formalin and euthanized. Brains were post-fixed, cryosectioned at 50 µm, and stained with DAPI (DAPI Fluoromount-G Mounting Media; SouthernBiotech (7)) for assessment of electrode placement (**Fig. S13**).

To characterize the extent of V1 viral transduction with Arch-GFP, four *Ntsr1-cre* mice were transduced as described above. After a 3-week period to allow for virally-mediated transgene expression, mice were perfused with 4% paraformaldehyde in ice cold 0.1M phosphate buffered saline. Brains were post-fixed and cryosectioned at 50 µm. Coronal sections through V1 were stained with mouse anti-NeuN (MAB377; 1:500; Millipore (8))

and secondary goat anti-mouse IgG1 594 (A-21125; 1:1000; Thermo Fisher Scientific (9)). Images were collected for all brain slices containing virally-transduced visual cortical regions. A region of interest was drawn around V1 L6 on each coronal slice using ImageJ software. Within this region, both the total number of NeuN+ L6 cells, and the number of NeuN+/GFP+ neurons was counted. Quantification of the proportion of V1 L6 neurons expressing GFP was independently verified by two scorers (**Fig. S9**). For characterization of ChR2-GFP expression, four *Ntsr1::ChR2* mice were perfused with 4% paraformaldehyde, and brains were post-fixed, sectioned, and stained for NeuN as described above. Quantification of the proportion of L6 V1 cells expressing GFP was carried out as described above (**Fig. S7A-B**).

Single unit discrimination

Single-neuron data were discriminated offline using standard principle component-based procedures as described previously (2, 10, 11) (**Fig. S4**). Briefly, spikes from individual neurons were discriminated on the basis of spike waveform shape and width, relative spike amplitude on the two stereotrode recording wires, and relative positioning of spike waveform clusters in three-dimensional principal component space. Single-neuron isolation was verified using standard techniques (12). Clusters with interspike interval (ISI)-based absolute refractory period violations were eliminated from analysis. Waveform cluster separation (for channels with more than one discriminated single unit) was first validated using MANOVA on the first 3 principal components ($p < 0.05$ for all sorted clusters; mean p value = 0.02 ± 0.01), and further characterized using the Davies-Bouldin (DB) validity index (a metric with inter-cluster distance as the

denominator, thus lower values indicate better cluster separation)(13). The mean (± SEM) DB value for all sorted waveform clusters (across all groups) was 0.32 ± 0.03, which compares favorably with DB values from single-unit data used in other studies(14, 15). Only those neurons that 1) met the criteria described above and 2) were reliably discriminated and continuously recorded throughout each experiment (*i.e.*, those stably recorded across both 24-h baseline and 12-h experimental condition) were included in firing rate analyses from behaving mice. For multielectrode recording from anesthetized mice, only those neurons reliably discriminated and stably recorded across baseline and optogenetic inhibition conditions were included in subsequent analyses.

Data analysis

Intracortical LFP and nuchal EMG signals were used to categorize each 10-s interval of recording as either REM, NREM, and wake (**Fig. S5A**), using custom data visualization software. For analyses of changes in LGN and V1 firing rate or spike-field coherence (SFC), only visually responsive neurons (assessed using criteria described above) were included. Firing rate and power spectral density were calculated separately within REM, NREM, and wake using NeuroExplorer software (Plexon). SFC was calculated by bandpass filtering LFPs corresponding to stably-recorded neurons, for either delta (0.5-4 Hz) or spindle (7-15 Hz) frequencies. Spike and LFP data were aligned and a spike triggered average was calculated for each neuron's spike trains (10). For normalization purposes (*i.e.*, for comparing SFC changes between experimental groups), these data were z-scored by randomizing spike times 100 times relative to LFPs, over a time window of up to 20 s (for delta) and 1.43 s (for spindle) (**Fig. 3B**). SFC raw values and

z-scores were then measured as changes from baseline in control conditions and laser-NREM conditions and compared via two-way RM ANOVA (**Fig. 5E**). Coherence between LGN and V1 LFPs was quantified in MATLAB. Briefly, LFPs from LGN were aligned to a reference LFP in V1, the LGN LFP was moved in time relative to the V1 LFP (± 200 ms and ± 100 ms lag time, respectively, for delta and spindle frequencies), and correlations between the fields were calculated at each lag time. Changes in peak correlation amplitude from baseline were compared between rest and laser-NREM conditions using Mann Whitney rank sum test (**Fig. 5C; Fig. S12A**). Changes in lag times between V1 and LGN fields were plotted as a cumulative probability distribution and assessed by Komlogorov-Smirnov test (**Fig. 5D; Fig. S12B**). For analysis of spindle occurrence during optogenetic stimulation experiments (**Fig. S8**), V1 LFPs were band-pass filtered at 11-15 Hz. Spindle-like events were defined as ≥ 6 successive deviations (i.e., peaks or troughs) of filtered signal that surpassed mean signal amplitude by 1.5 standard deviations.

Wilcoxon signed rank tests were used to assess firing rate changes over stimulus presentation, (**Fig. 2C**). Correlations between firing rate changes, spike field coherence, and visual response properties were assessed by Pearson product moment, and fit with a linear regression (**Figs. 2B,D & 3C**). All measures of change induced by optogenetic manipulation in **Fig. 5** were expressed as a change from baseline values (i.e., experimental – baseline). For analysis of power spectral density, Student's t-tests were conducted at each frequency bin from 0-15 Hz (n = 76 bins) and a Bonferroni correction for multiple comparisons was applied to the results (**Fig. 5B**). Area under the curve was

calculated for delta (0.5-4 Hz) and spindle (7-15 Hz) frequency bins to assess changes in power at these frequencies (**Fig. 5B**).

To ensure state-specific optogenetic manipulation had no effect on sleep architecture, a 2-way ANOVA was used to quantify proportions of time spent in each state (factor A: experimental condition, factor B: time of day; **Fig. S17**). Effects of state-specific optogenetic inhibition of CT neurons were assessed by 1-way RM ANOVA (**Fig. 6B**).

To address potential confounds from nested data, within-mouse averages were generated for data in **Figs. 1C, 2B, 2D, 3B, 3C, and 6B.** These values are now plotted in **Figs. S1B, S6A, S6B, S6C, S6D, & S20B**, respectively.

Data and code availability

Raw data files will be shared by the Aton lab in response to reasonable requests to the corresponding author. Custom MATLAB code for quantifying visual responses and for calculating and normalizing SFC (from spike sorted .nex files) will be made available for free download on the Aton lab website: https://sites.lsa.umich.edu/aton-lab/.

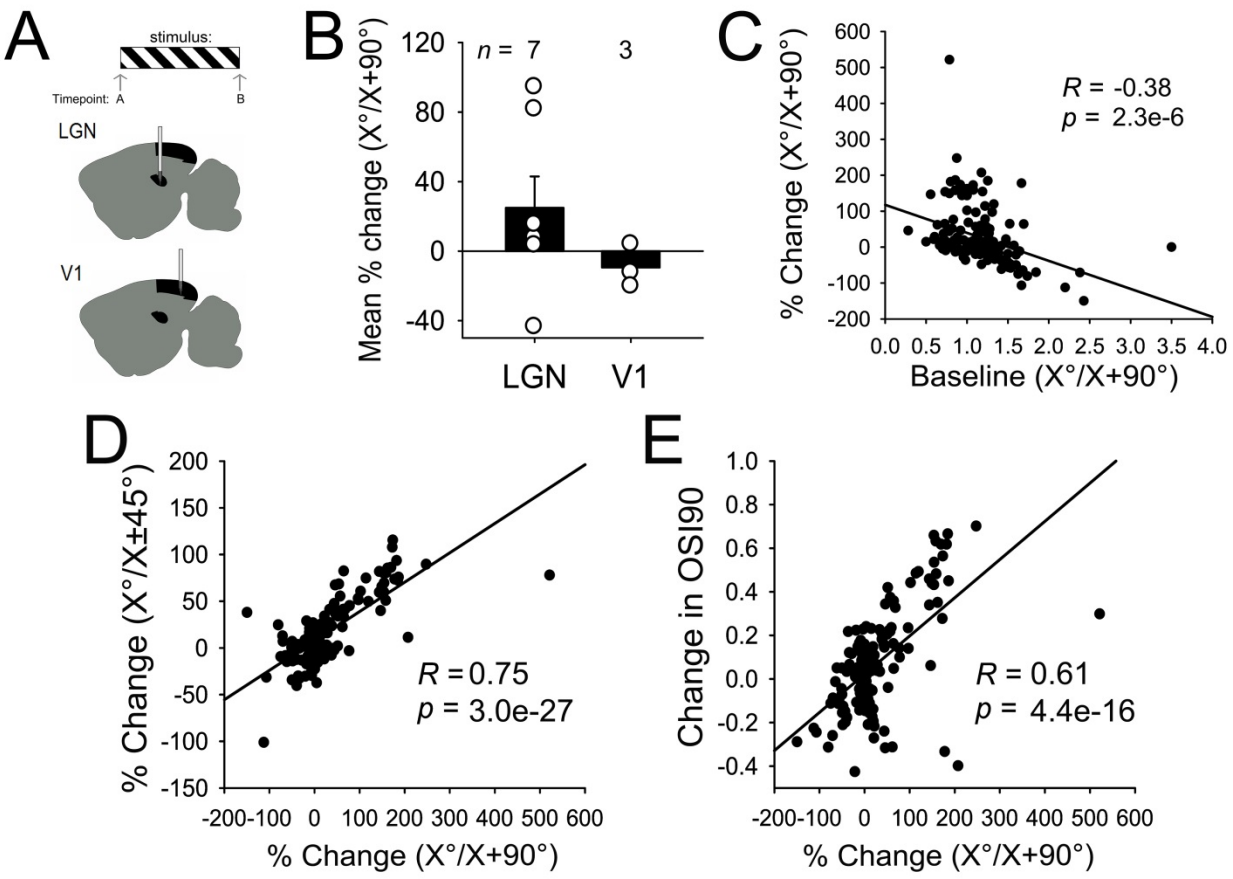

Figure S1 - Features of OSRP expressed by LGN neurons after visual stimulus presentation. A) Experimental design for anesthetized recordings, as described in **Fig. 1A**. **B**) Changes in the responsiveness to the presented oriented grating stimulus (vs. orthogonal orientation) averaged across LGN or V1 for each mouse. These average changes were highly variable in LGN, but generally followed the same trend as shown in **Fig. 1C**. **C**) Among LGN neurons, the degree of OSRP (change in [X°/X+90°]) after stimulus presentation was inversely related to baseline (X°/X+90°) ratio. The extent of OSRP in individual LGN neurons was positively correlated with **D**) relative increases in responsiveness to the presented orientation vs. oblique orientations and **E)** orientation selectivity (OSI90) increases. Pearson product moment *R* and *p* values are shown for 147 LGN neurons.

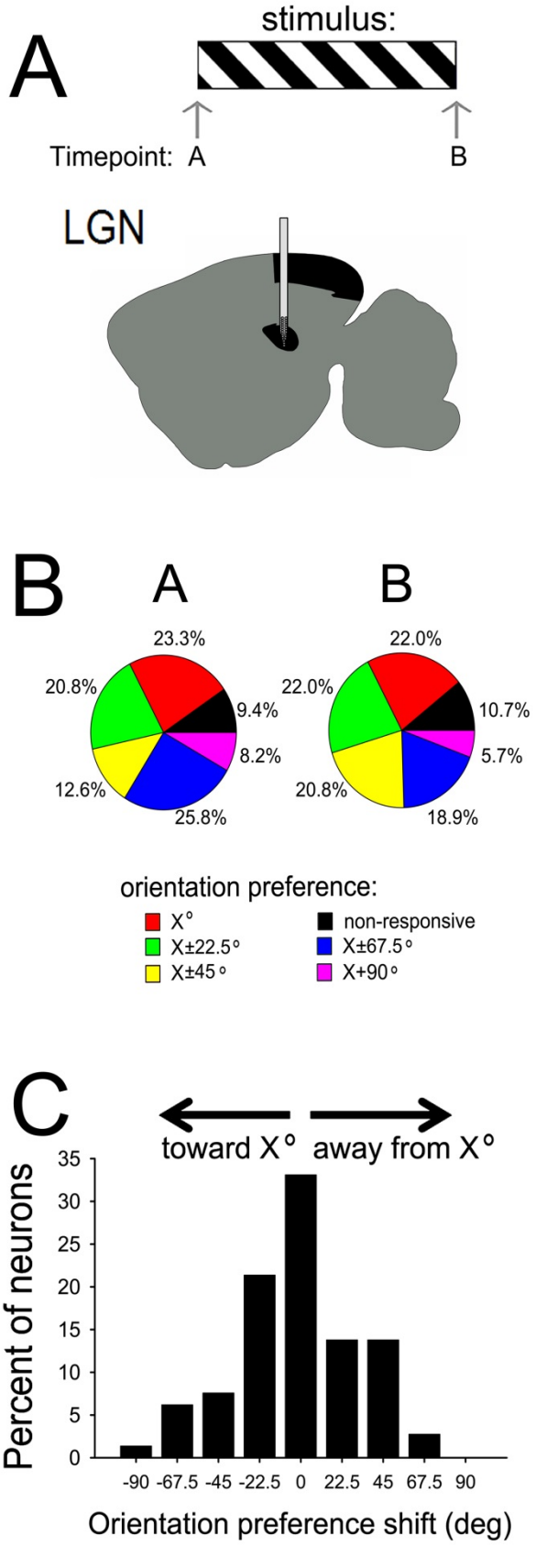
A
stimulus:
Timepoint: A
B
LGN
B
A
B
23.3%
20.8%
9.4%
8.2%
12.6%
25.8%
22.0%
22.0%
10.7%
5.7%
20.8%
18.9%
orientation preference:
X°
X±22.5°
X±45°
non-responsive
X±67.5°
X+90°
C
toward X°
away from X°
Percent of neurons
35
30
25
20
15
10
5
0
-90 -67.5 -45 -22.5 0 22.5 45 67.5 90
Orientation preference shift (deg)

Figure S2 – Distribution of orientation-specific responses in LGN neurons, and changes in orientation preference across stimulus presentation. A) Schematic of LGN neuronal recordings from anesthetized mice as described in **Fig. 1A**. **B)** Distributions of orientation preference among visually responsive LGN neurons (and proportions of non-responsive neurons) before (timepoint A) and after (timepoint B) stimulus presentation. OSRP measured across stimulus presentation in LGN was not associated with an increase in the proportion of LGN neurons preferring the stimulus (X°) orientation, although the proportions of neurons preferring the orthogonal (X+90°) and X±67.5°orientations were reduced slightly. **C)** Distribution of the changes in preferred orientation for individual LGN neurons across stimulus presentation. Data are presented for all visually responsive neurons. 0 indicates no change, while negative and positive shifts, respectively, indicate shifts in response preference toward and away from the presented stimulus orientation.

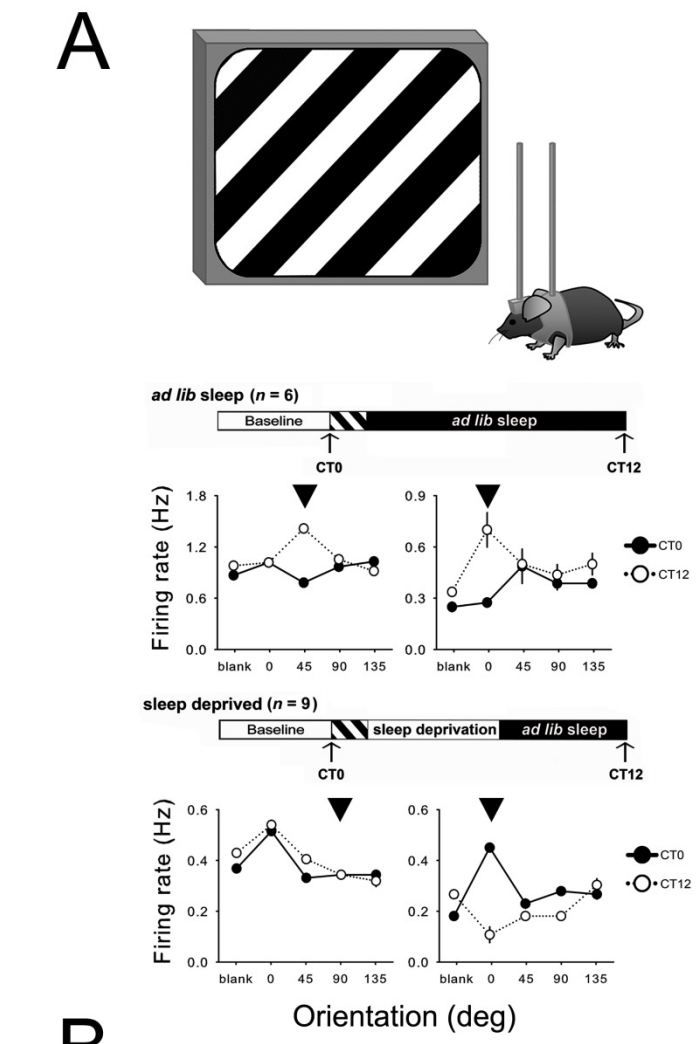

Figure S3 - Orientation-specific response potentiation (OSRP) in V1 is sleep-dependent. A) Schematic of OSRP experiment. Mice were implanted with V1 stereotrodes for continuous

recording of neurons and local field potentials. At CT0, following a 24-h baseline recording period, mice were temporarily head-fixed and shown a series of oriented gratings (0, 45, 90, and 135 degrees) to measure V1 neurons' baseline visual response properties (first black arrow). One grating of a single orientation was then selected for 30-min presentation, to induce ORSP. Following stimulus presentation, mice were either allowed *ad lib* sleep, or were sleep deprived for the first 6 h by gentle handling. At CT12, visual response properties were reassessed (second black arrow). Tuning curves at CT0 and CT12 (black and white respectively) for 2 representative neurons recorded from a C57BL/6J mouse allowed *ad lib* sleep, and for 2 representative neurons recorded from a sleep deprived mouse. Values indicate mean firing rate response for each stimulus, ± SEM. *n* indicates the total number of mice recorded in each condition. Arrowheads indicate the orientation of the grating presented over 30 min to induce OSRP. **B)** OSRP is calculated as % change in the ratio of firing rate responses to stimuli of the presented and orthogonal orientation between CT0 and CT12. Analysis is shown for individual neurons (left) and averaged values for each mouse (right). Following *ad lib* sleep, V1 neurons show a significant increase in preference for the presented stimulus orientation (arrowhead indicates $p < 0.05$, RM ANOVA on ranks), which is not seen in sleep deprived mice (* indicates $p < 0.05$ for *ad lib* sleep vs. sleep deprived). *n* indicates the total number of neurons recorded in each condition.

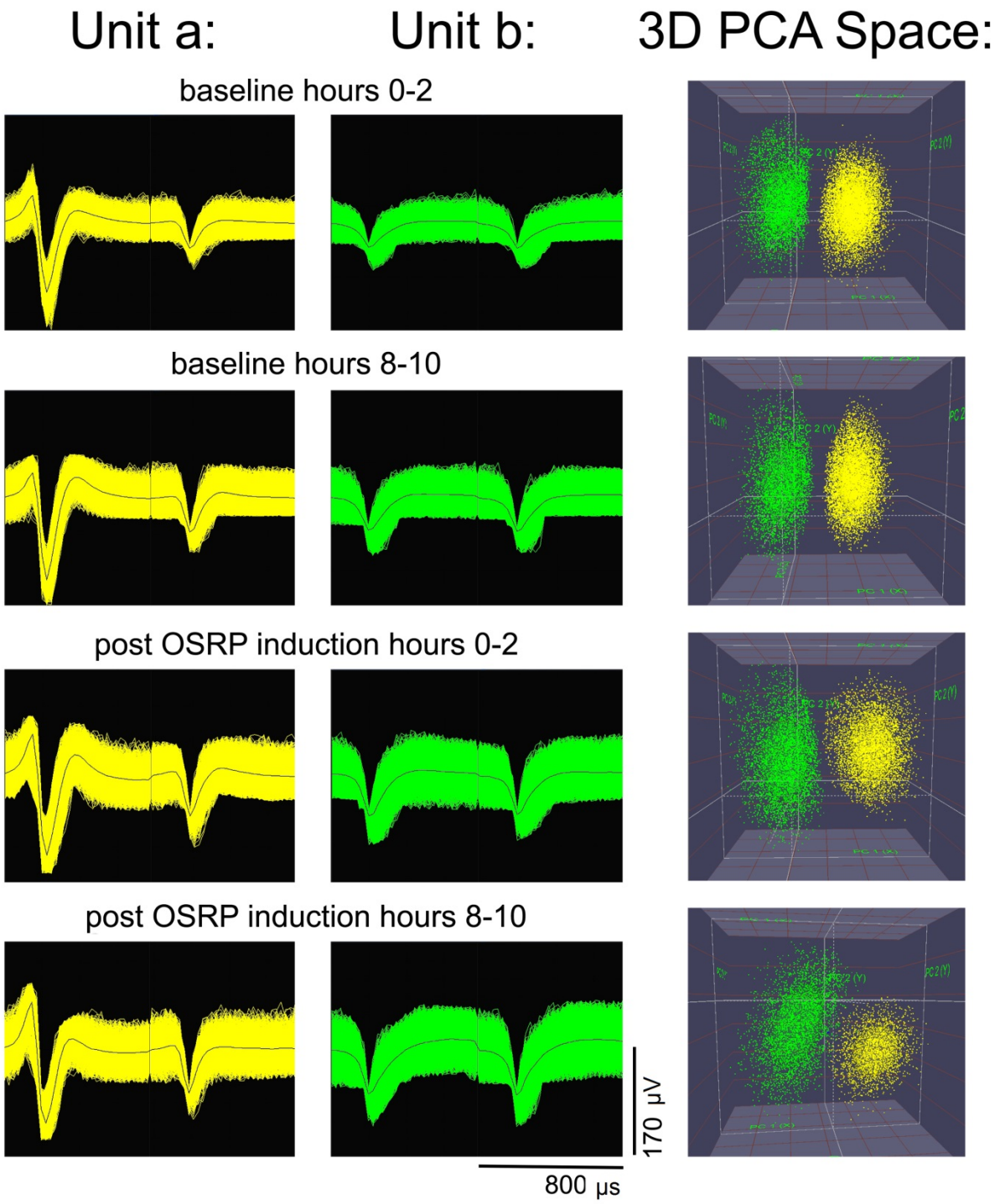

Figure S4 - Spike sorting and spike cluster stability over time. Left: Spike waveforms for 2 representative neurons recorded on the same stereotrode across 2-h windows at baseline, and following stimulus presentation on the second day of recording. Right: Clusters of spike

waveforms in 3-dimensional principal component space. For all recordings, cluster separation was validated using MANOVA ($p < 0.05$ for all sorted clusters; mean p value = 0.02 ± 0.01), and further characterized using the Davies-Bouldin (DB) validity index (mean DB index = 0.32 ± 0.03).

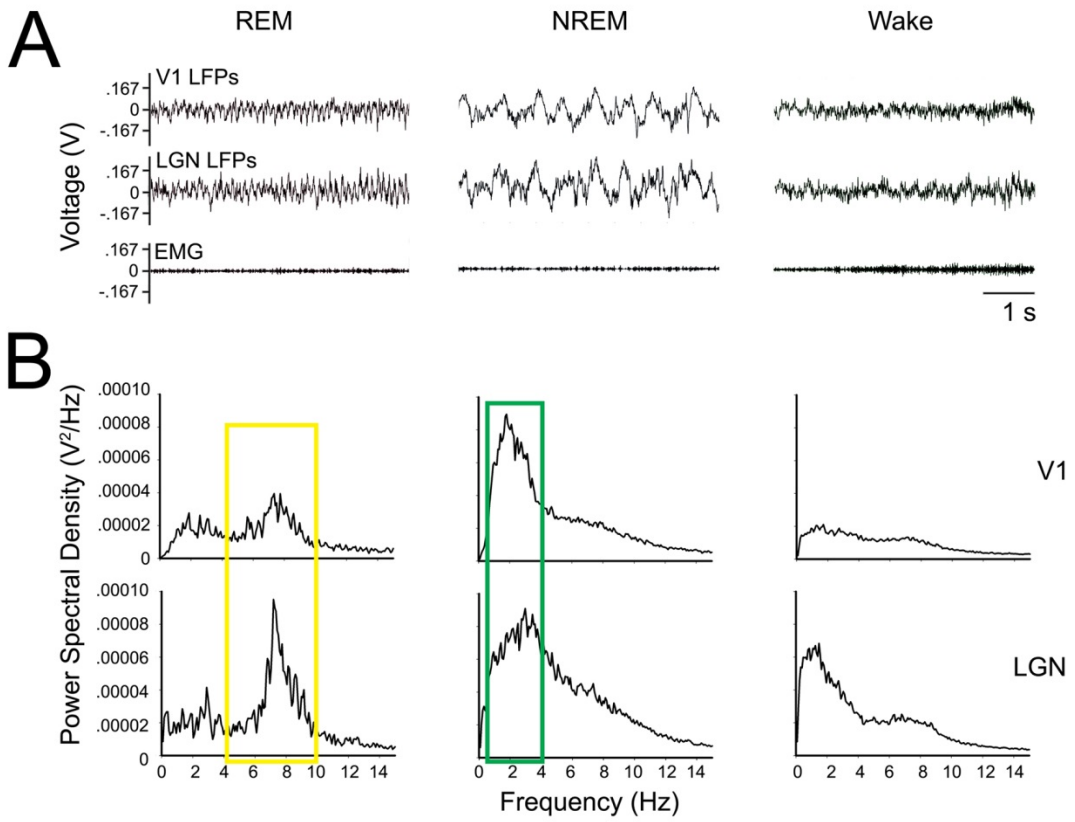

Figure S5 - Representative LFP and EMG data used for sleep scoring. A) Representative V1 (top) and LGN (middle) LFPs and EMG (bottom) traces during REM sleep (left), NREM sleep (middle), and wake (right). **B)** Power spectral density (PSD) graphs for V1 (top) and LGN (bottom). REM sleep is characterized by high theta frequency (4-10 Hz) activity (highlighted in yellow) in the LFP and low EMG activity. NREM sleep is characterized by high amplitude delta frequency (0.5-4 Hz) activity (highlighted in green) in the LFP and low EMG activity. Wake is characterized by low amplitude LFP activity and higher, more variable EMG activity.

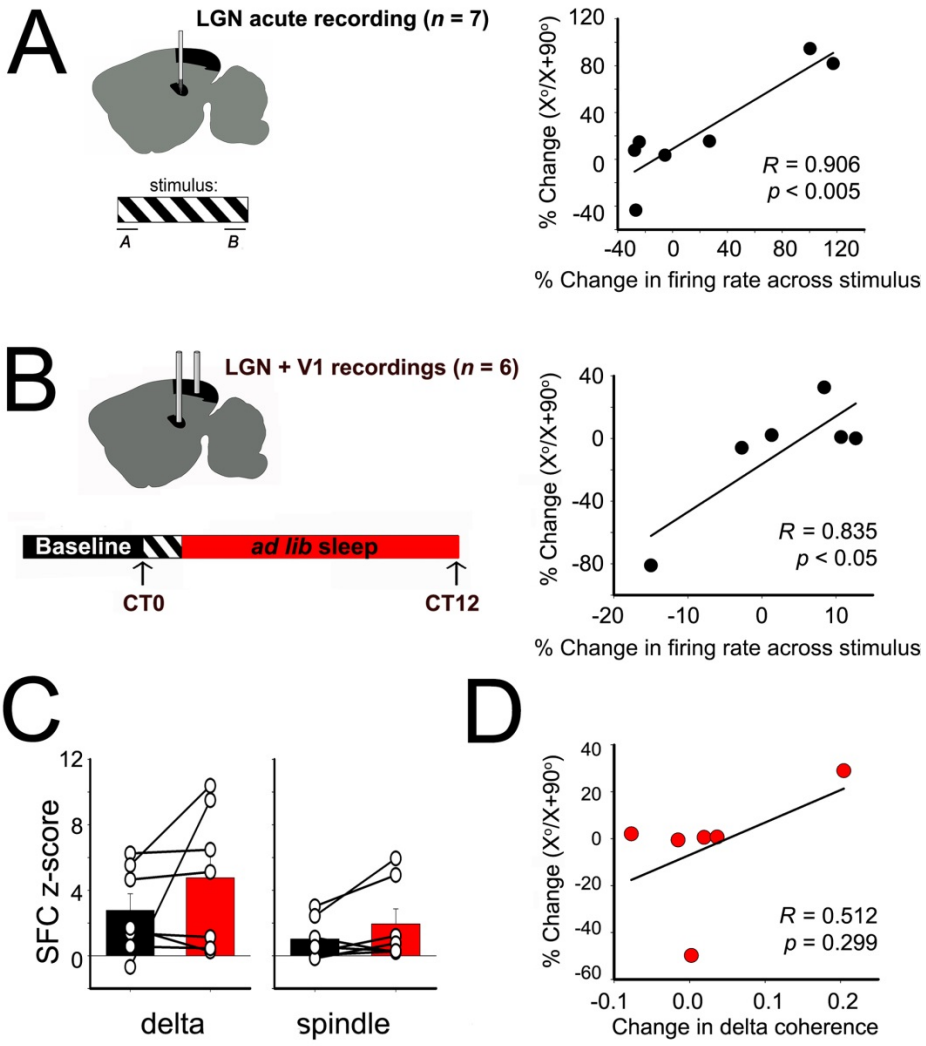

Figure S6 - Changes in neuronal firing properties induced by stimulus presentation predict OSRP. A) Left: Schematic of anesthetized LGN recording. **Right:** The mean values from each mouse with data presented in **Fig. 2B** are shown. Per animal mean LGN neuron firing rate changes over stimulus presentation predict mean per animal OSRP measures (*R* and *p* values are shown for Pearson product moment). **B) Left:** Schematic of chronic recording in mice implanted with LGN and V1 stereotrodes. **Right:** Per animal means of firing rate data from **Fig. 2D.** There is a similar, significant relationship between mean LGN neuron firing rate changes

and mean OSRP per animal (*R* and *p* values are shown for Pearson product moment). **C)** Per animal means of SCF data from **Fig. 3B.** When averaged within each animal the changes in delta and spindle SFC are not significant (*N.S.,* Wilcoxon signed rank test). **D)** Per animal means of data in **Fig. 3C.** There is no significant relationship between the change in delta coherence and the % change in OSRP measurement when data is aggregated into averages per animal, although the trend is similar to that shown for **Fig. 3C** (*N.S.,* Pearson product moment).

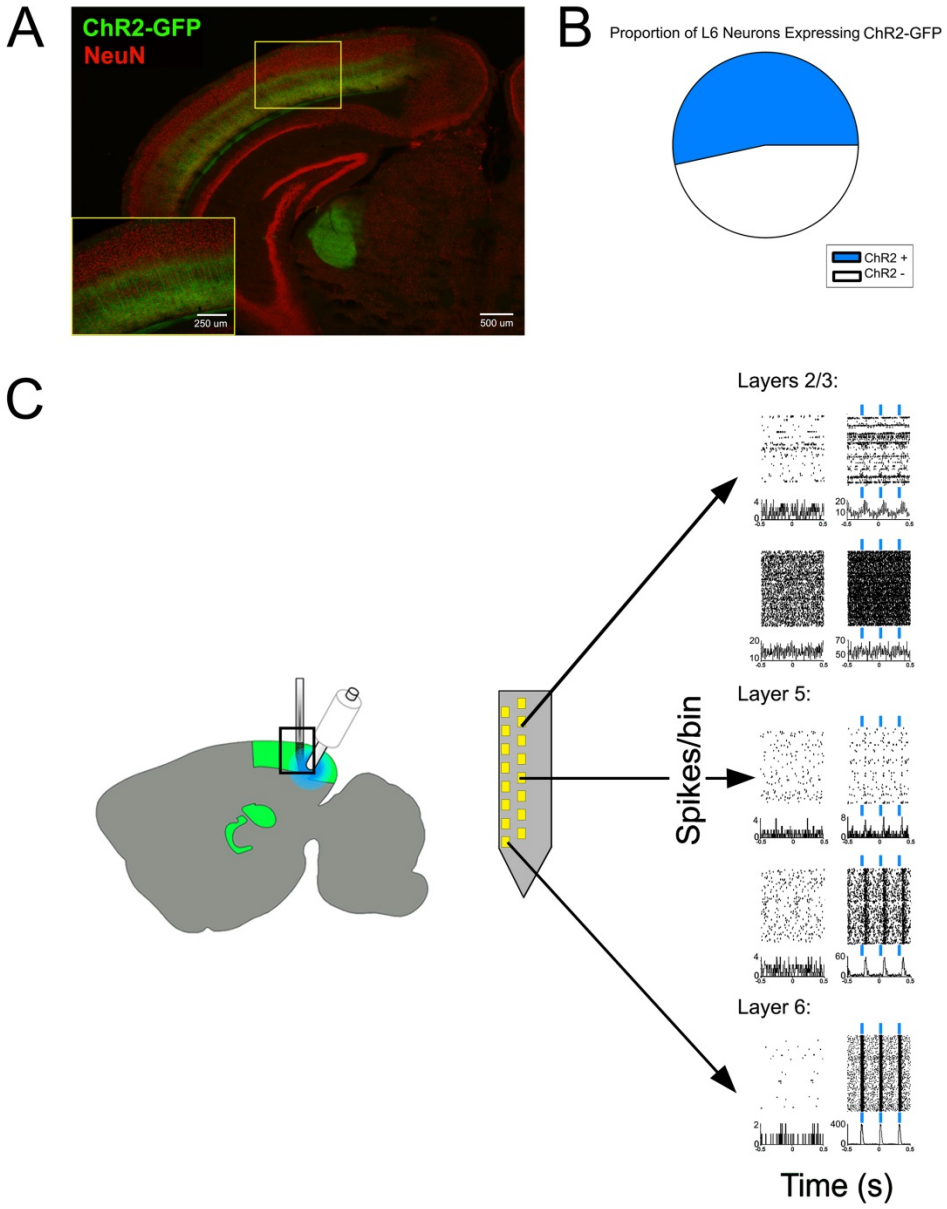

Figure S7 - ChR2-GFP expression in V1 L6 neurons and recording during optogenetic stimulation. A) GFP expression in V1 L6 neurons of *Ntsr1::ChR2* crossed transgenic mice. Wide field images show axon termini in thalamic nuclei, inset shows cell bodies in V1. **B)** Histological assessment of *n* = 4 transgenic mice showed ChR2-GFP expression in 53.4 ± 1.5% of all NeuN+

V1 L6 neuronal cell bodies (a similar proportion to the number of L6 neurons which project to thalamus (16)). **C)** Schematic of recording of neuronal activity during optogenetic stimulation in *Ntsr1::ChR2* mice. Linear probes with 25 um spacing between sites allowed for recording of multiple cortical layers across V1 simultaneously. Representative data are shown for neurons simultaneously recorded across V1 layers during optogenetic stimulation. Only within L6 (where neurons were directly activated by light delivery) was neuronal spiking precisely timed to light pulses.

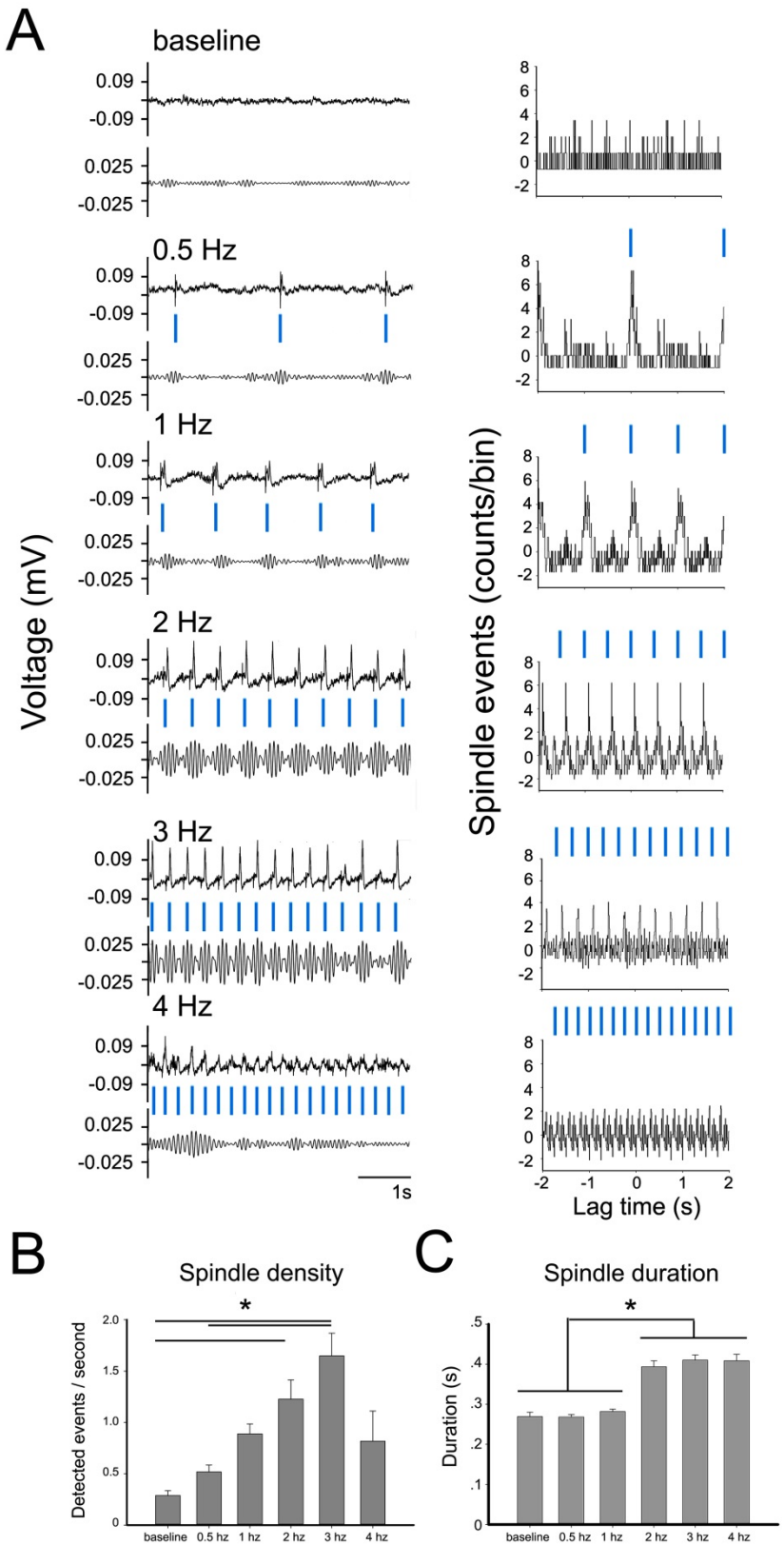
A
baseline
0.5 Hz
1 Hz
2 Hz
3 Hz
4 Hz
Voltage (mV)
0.09
-0.09
0.025
-0.025
1s
Spindle events (counts/bin)
Lag time (s)
B
Spindle density
Detected events / second
baseline
0.5 hz
1 hz
2 hz
3 hz
4 hz
C
Spindle duration
Duration (s)

Figure S8 - Stimulation of V1 L6 neurons induces sleep spindle-like oscillation in V1. A) Left: Representative raw and filtered (11-15 Hz) LFPs recorded from V1 at baseline (in the absence of light delivery to V1), and during optogenetic stimulation of L6 neurons at a range of frequencies. **Right:** An automated spindle detection algorithm (see SI Materials and Methods) was used to detect the occurrence of spindles. The timing of spindle occurrence is shown relative to timing of light delivery to V1. **B)** Frequency of occurrence for spindle-like events (mean ± SEM) at baseline and during optogenetic stimulation. The density of spindle-like events was significantly increased during optogenetic stimulation at 2 Hz and 3 Hz (one-way ANOVA; * indicates $p < 0.05$, $p < 0.005$, and $p = 0.01$ for 2 Hz vs. baseline, 3 Hz vs. baseline, and 3 Hz vs. 0.5 Hz, Holm-Sidak *post hoc* test). **C)** Durations of spindle-like events (mean ± SEM) elicited by optogenetic stimulation of L6 neurons at various frequencies, and under baseline conditions without stimulation (one-way ANOVA on ranks; * indicates $p < 0.001$, Dunn's Method *post hoc*).

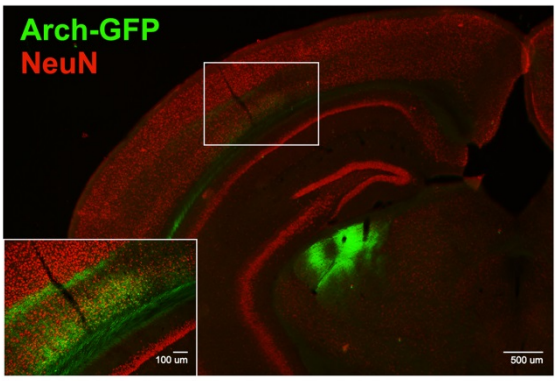

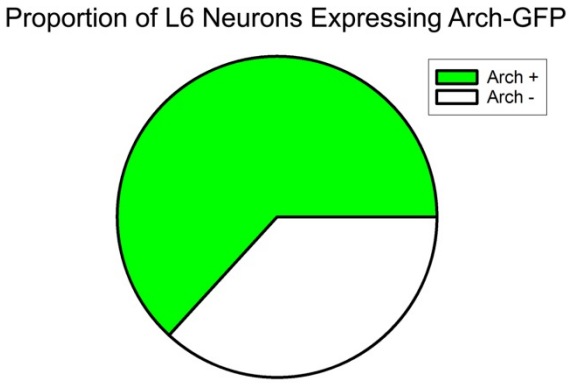

Figure S9 - Arch-GFP expression in V1 L6 neurons. Left: GFP expression in V1 L6 neurons of virally-transduced *Ntsr1-cre* transgenic mice. Wide field image shows axon termini in LGN, inset shows cell bodies in L6. **Right:** Histological assessment of *n* = 4 transduced mice showed Arch-GFP expression in 63.2 ± 1.6% of all NeuN+ V1 L6 neuronal cell bodies (a similar proportion to the number of L6 neurons which project to thalamus (16)).

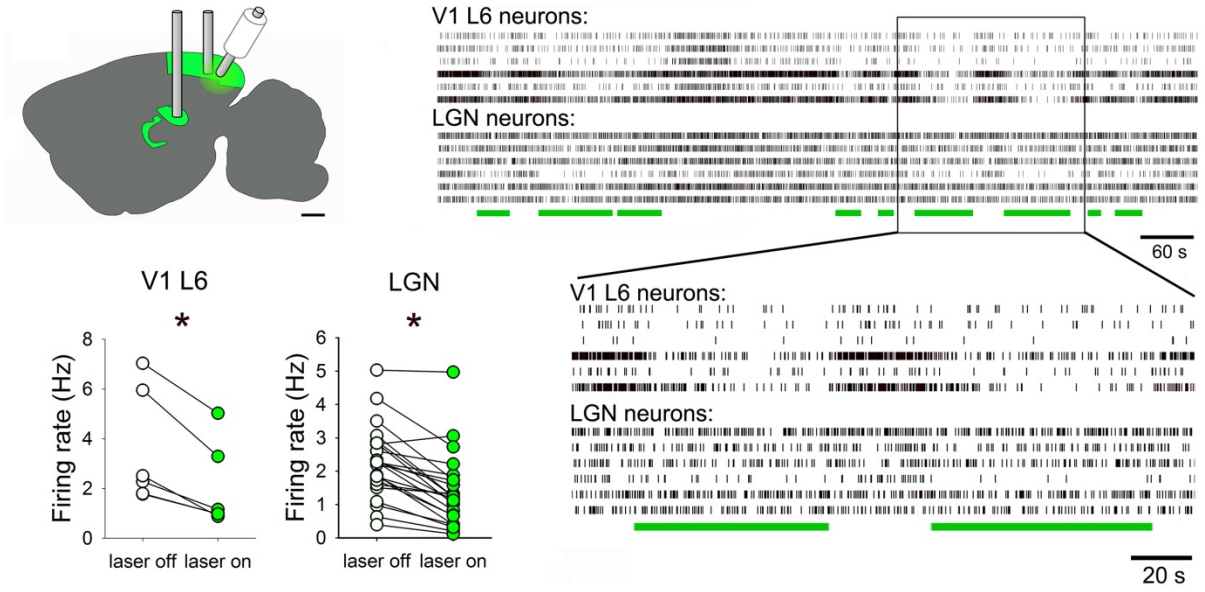

Figure S10 - Optogenetic inhibition of L6 CT neurons in freely-behaving mice. Top, left: Experimental schematic, showing placement of stereotrode bundles for continuous, simultaneous recording of LGN and V1 neuronal activity in Arch-GFP-transduced *Ntsr1-cre* transgenic mice. **Top, right:** Spike rasters for simultaneously-recorded L6 and LGN neurons during optogenetic inhibition (laser light delivery times indicated by green bars). **Bottom, left:** Light delivery led to a significant reduction in both V1 L6 neurons' (n = 6) and LGN neurons' (n = 23) firing rates. * indicates $p < 0.005$, Wilcoxon signed rank test. **Bottom, right:** Inset from longer spike raster above.

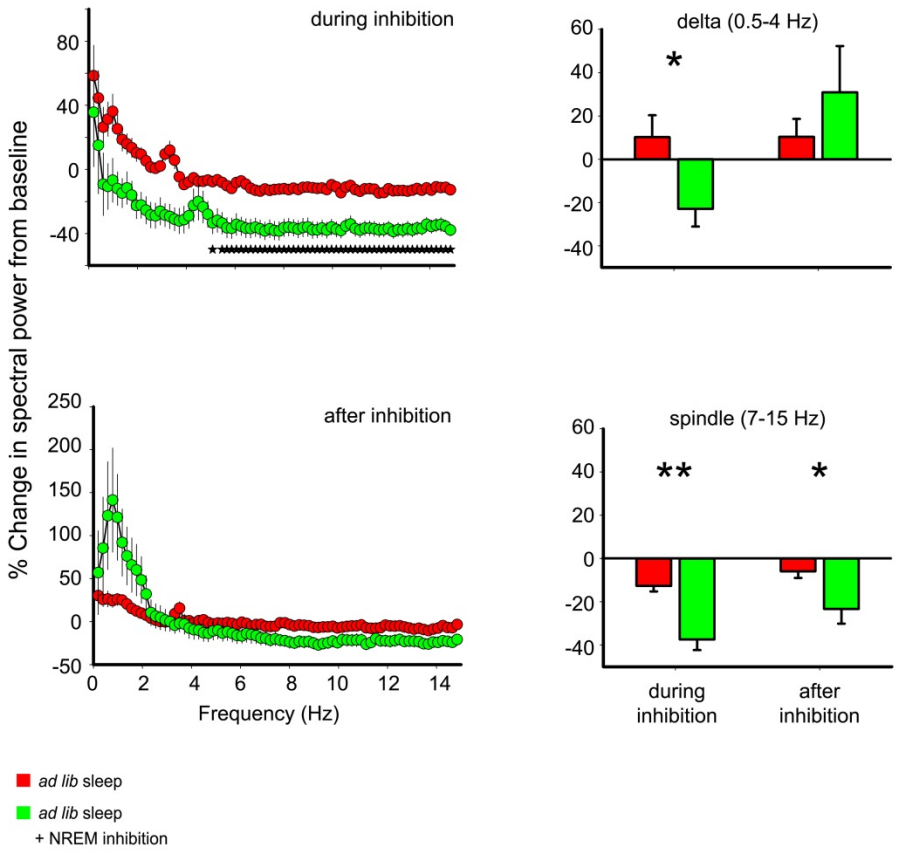

Figure S11- Power spectral changes during NREM-inhibiton of CT neurons as a percent change from baseline. Left: During the 6 hours following OSRP induction, percent change in spectral power from baseline was significantly different between *ad lib* sleep mice and NREM-specific inhibition mice (*$p < 0.05$, t-test after Bonferroni correction). No significant differences were detected following the inhibition period. **Right:** Percent changes from baseline in summed spectral power at delta (**top**) and spindle (**bottom**) frequencies were calculated for *ad lib* sleep and NREM inhibition conditions. Percent change in summed delta power was significantly more negative for NREM inhibition LFPs versus control LFPs during inhibition, but not after ($p = 0.015$ and $p = 0.337$, respectively; t-test). Percent change in summed spindle power was significantly more negative for NREM inhibition LFPs versus control LFPs during and after inhibition ($p = 0.0000054$ and $p = 0.0135$, respectively; t-test). *$p < 0.05$ and **$p < 0.0001$.

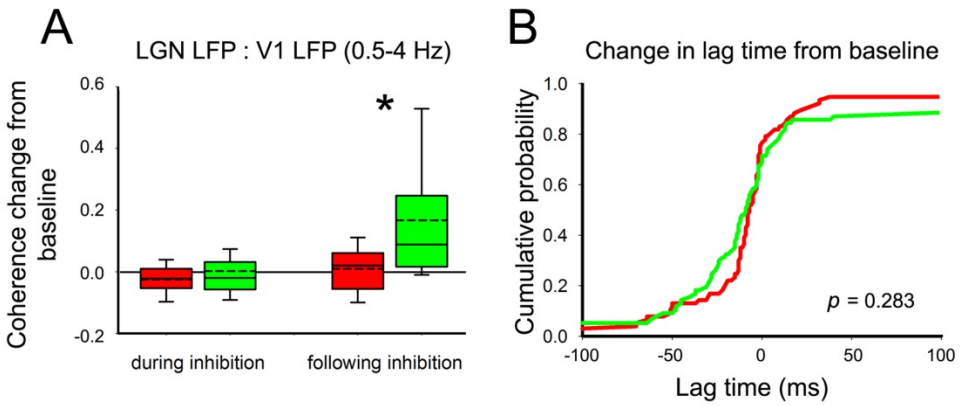

Figure S12 - NREM delta-frequency coherence between V1 and LGN LFPs under control and optogenetic inhibition conditions. A) Delta-frequency coherence between V1 and LGN LFPs was not significantly affected during NREM-specific inhibition of L6 CT neurons, but was increased relative to no laser control conditions after the inhibition period (p = 0.418 and p < 0.001, respectively; Mann-Whitney rank sum test). **B)** For delta-frequency activity, there was no shift in the time lag between LGN and V1 LFPs (relative to baseline) with NREM-targeted inhibition of CT neurons (p = 0.283, Kolmogorov-Smirnov test vs. no laser condition).

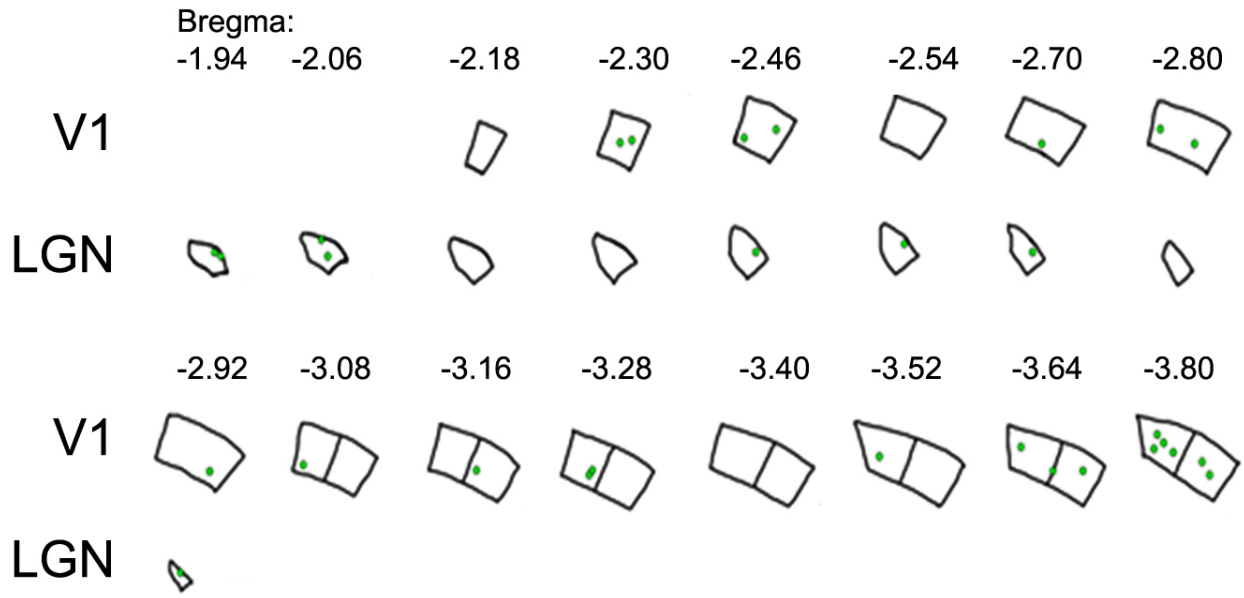

Figure S13 - LGN and V1 recording sites. Locations of stereotrode recordings in all experiments from freely-behaving mice. Anterior-posterior position in coronal sections relative to bregma (in mm) shown in LGN, monocular and binocular right-hemisphere V1.

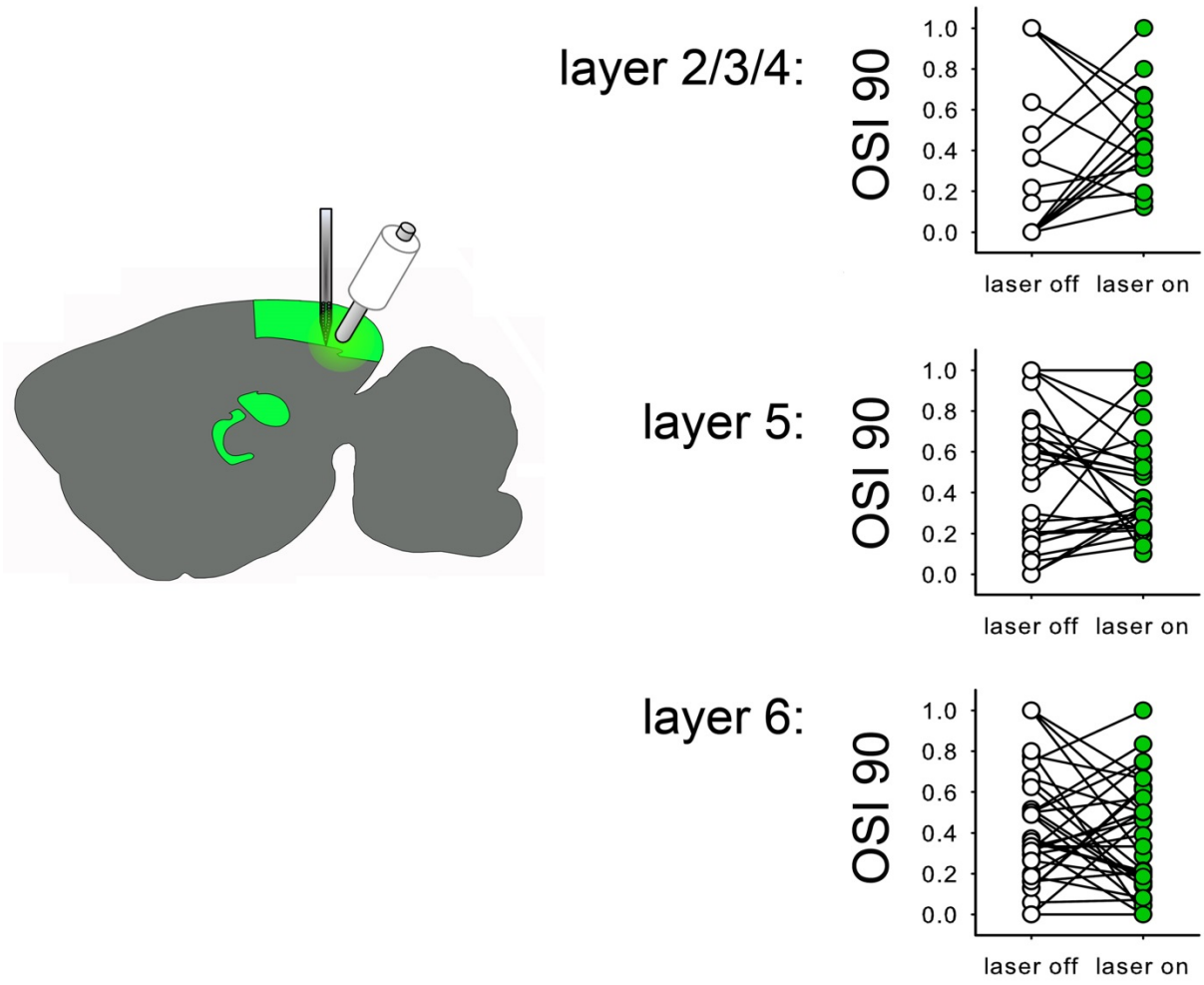

Figure S14 - Direct effects of optogenetic inhibition of L6 CT neurons on V1 orientation tuning. V1 response properties recorded in anesthetized Arch-GFP-transduced mice before and during optogenetic inhibition of CT neurons (*n* = 24 neurons from layer 2/3/4, *n* = 32 neurons from layer 5, and *n* = 38 neurons from L6, recorded from *n* = 5 mice). Neuronal orientation tuning was not significantly or consistently altered in any layer by optogenetic inhibition (*N.S.* for all layers, Wilcoxon signed rank test).

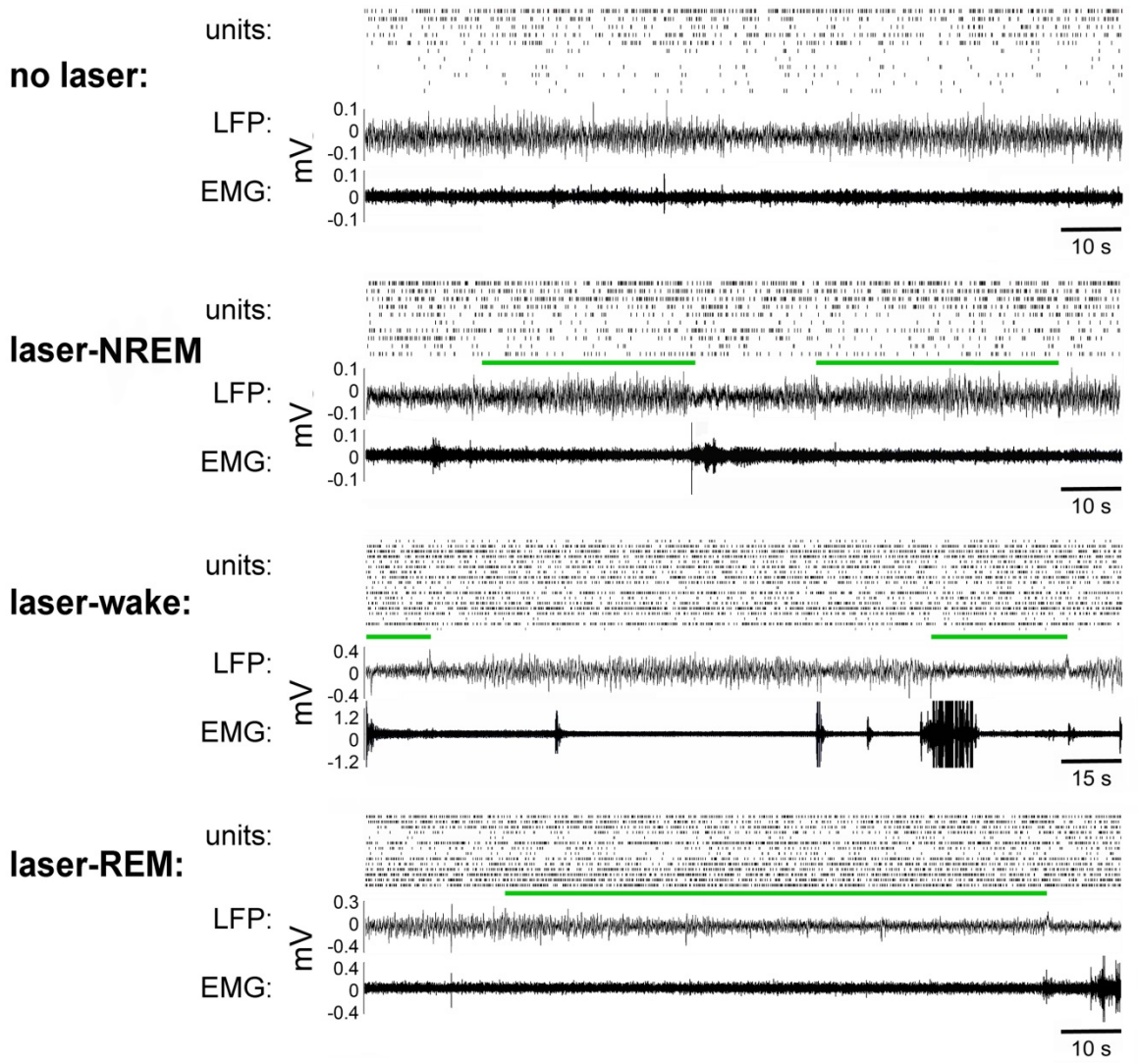

Figure S15 - Electrophysiological activity recorded during state-specific inhibition of L6 CT neurons. Representative examples V1 spike rasters, V1 LFPs, and EMG activity during state-targeted inhibition of L6 neurons. Laser on times are indicated with green bars below rasters.

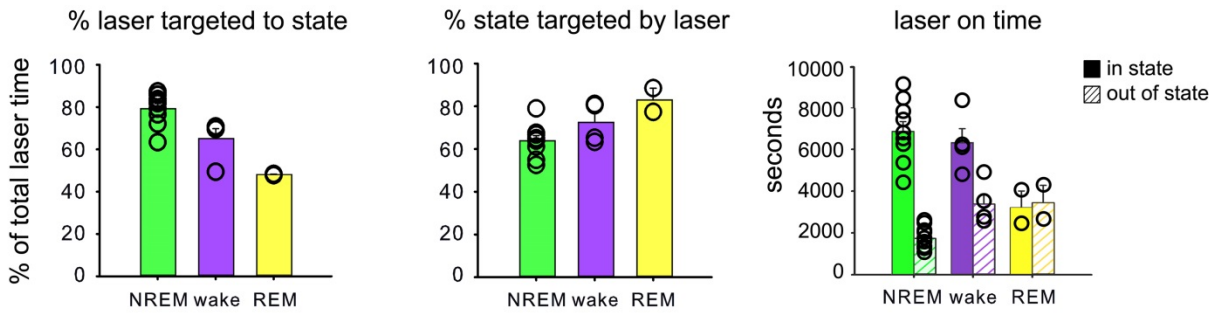

Figure S16 - State targeting of inhibition of L6 CT neurons. Left: Percent of laser on time accurately targeted to state in laser-NREM (green) laser-wake (violet) and laser-REM (yellow) conditions. **Middle:** Percent of time in target state with laser on in the 3 conditions. **Right:** Laser on time (in s) for each condition, corresponding to time in and out of the targeted state, in the 3 conditions.

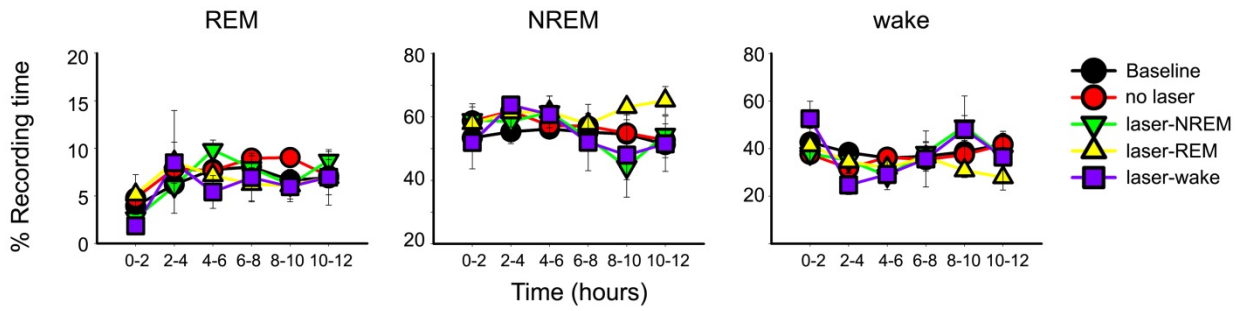

Figure S17 - Sleep architecture is unaffected by state-specific inhibition of L6 CT neurons. % time spent in (from left to right) REM, NREM, and wake, for mice in the various state-targeted optogenetic inhibition conditions. Values are presented in 2-h windows across the rest phase (CT0-12), corresponding to the *ad lib* sleep period between stimulus presentation and OSRP assessment. State-targeted inhibition had no significant effect on sleep architecture ($p = 0.161$, $p = 0.186$, and $p = 0.350$ for REM, NREM, and wake, respectively; 2-way RM ANOVA).

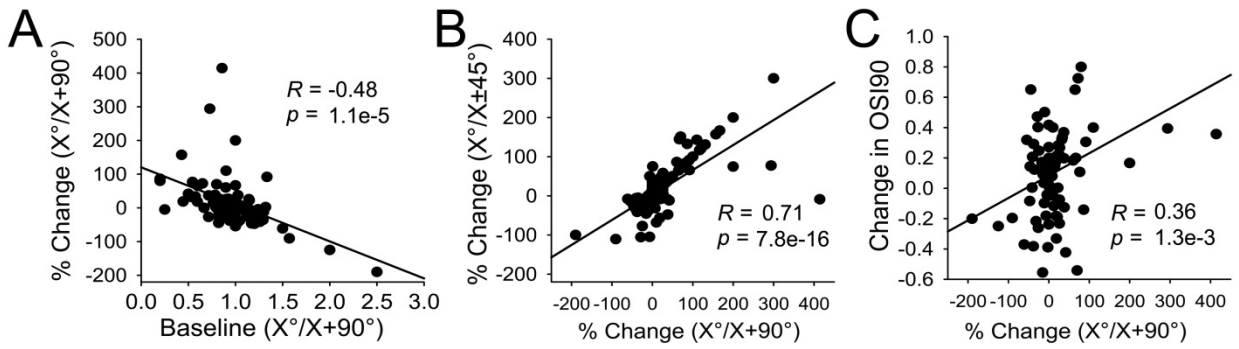

Figure S18 - Features of OSRP expressed by V1 neurons after a period of sleep. A) Among V1 neurons recorded from mice in the control (no laser) group, the degree of OSRP (change in [X°/X+90°]) after a period of sleep was inversely related to pre-stimulus baseline (X°/X+90°) ratio. The extent of OSRP in individual V1 neurons was positively correlated with **B**) relative increases in responsiveness to the presented orientation vs. oblique orientations and **C)** orientation selectivity (OSI90) increases (Pearson product moment). Pearson product moment *R* and *p* values are shown for 97 neurons.

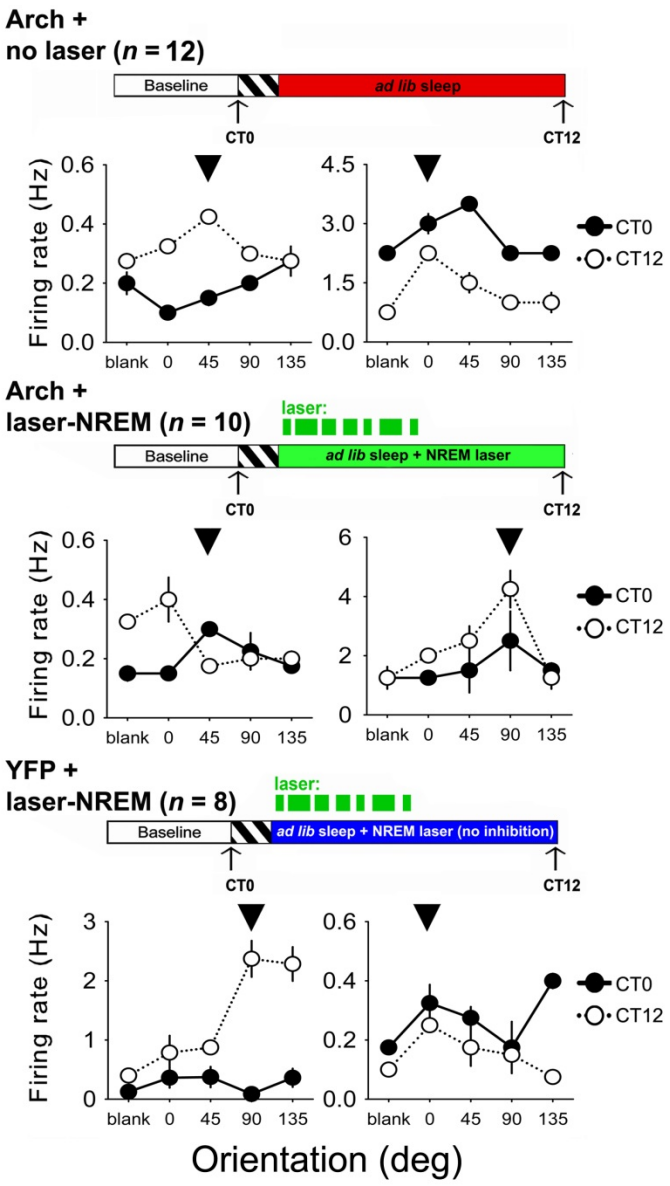

Figure S19 - Response property changes in representative V1 neurons. Representative tuning curves for V1 neurons recorded at baseline (CT0; black) and following post-stimulus sleep (CT12; white) for mice in no laser (top), laser-NREM (middle), and laser-NREM YFP control (bottom) conditions. Values indicate mean firing rate response for each stimulus, ± SEM. *n* indicates the total number of mice recorded in each condition. Arrowheads indicate the orientation of the grating presented over 30 min to induce OSRP.

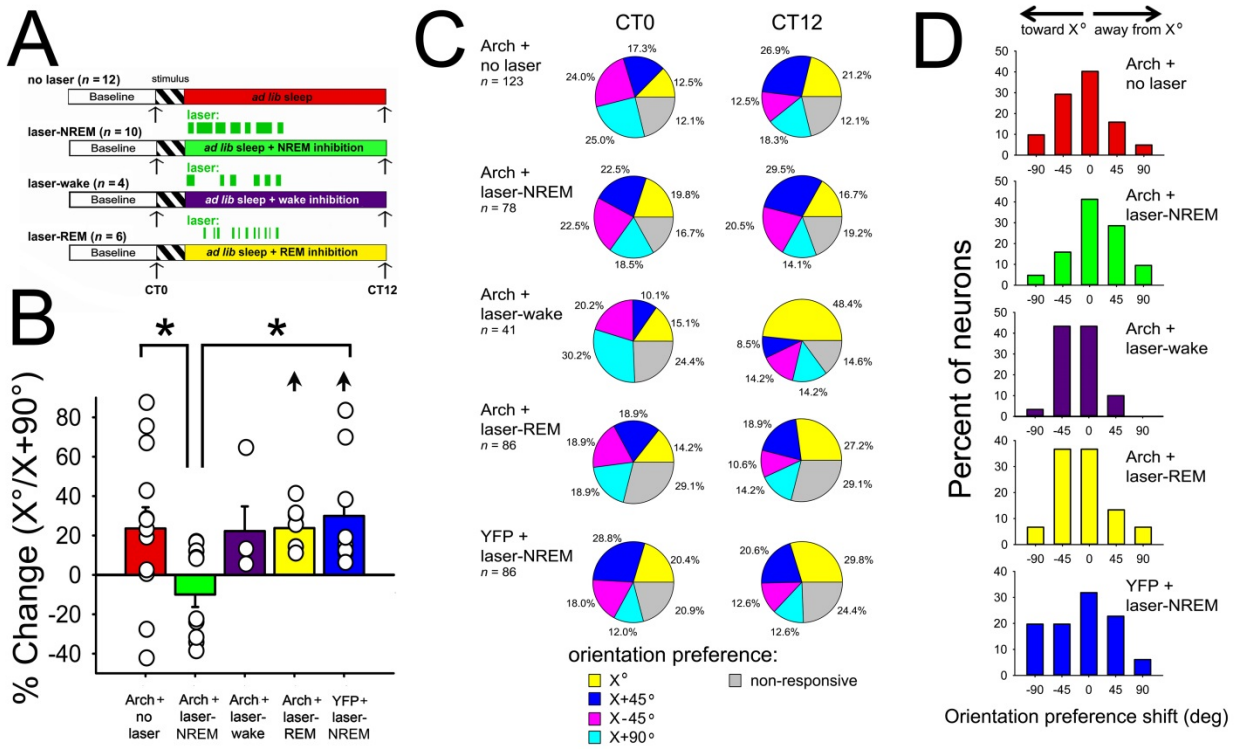

Figure S20 – Per animal averages of OSRP reflect changes at the individual neuron level. A) Experimental paradigm for evaluating the effects of post-stimulus state-targeted optogenetic inhibition of V1 CT neurons on OSRP consolidation. **B)** Mean OSRP measured within individual animals is shown for each of the treatment groups. NREM-targeted inhibition of V1 CT neurons (laser-NREM) reduced OSRP in V1, while inhibition in other states did not affect OSRP. * indicates $p < 0.05$, Dunn's *post hoc* test versus no laser controls and YFP-expressing control mice with light delivery targeted to V1 during NREM ($p < 0.001$; Kruskal Wallis ANOVA on ranks). Arrowhead indicates $p < 0.05$, RM ANOVA on ranks. **C)** Distributions of orientation preference among visually responsive V1 neurons (and proportions of non-responsive neurons) at baseline, and after a period of post-stimulus sleep. OSRP after a period of post-stimulus sleep was generally associated with an increase in the proportion of V1 neurons preferring the stimulus (X°) orientation, and a general reduction in the proportion of neurons preferring other

orientations. Such changes were present in all groups of mice, except those receiving NREM-targeted optogenetic inhibition of L6 neurons (where response distributions were virtually unchanged across the experiment). **C)** Distribution of the changes in preferred orientation for individual V1 neurons across stimulus presentation. Data are presented for all visually responsive neurons. 0 indicates no change, while negative and positive shifts, respectively, indicate shifts in response preference toward and away from the presented stimulus orientation. With the exception of mice receiving NREM-targeted optogenetic inhibition of L6 neurons, these distributions were skewed in favor of shifts toward the presented stimulus (X°).

Supplemental References:

1. Olsen SR, Bortone DS, Adesnik H, & Scanziani M (2012) Gain control by layer six in cortical circuits of vision. *Nature* 483(7387):47-52.
2. Aton SJ, Suresh A, Broussard C, & Frank MG (2014) Sleep promotes cortical response potentiation following visual experience. *Sleep* 37(7):1163-1170.
3. Durkin J & Aton SJ (2016) Sleep-Dependent Potentiation in the Visual System Is at Odds with the Synaptic Homeostasis Hypothesis. *Sleep* 39(1):155-159.
4. Aton SJ*, et al.* (2009) Mechanisms of sleep-dependent consolidation of cortical plasticity. *Neuron* 61(3):454-466.
5. Frenkel MY*, et al.* (2006) Instructive effect of visual experience in mouse visual cortex. *Neuron* 51(3):339-349.
6. Niell CM & Stryker MP (2008) Highly selective receptive fields in mouse visual cortex. *J Neurosci* 28(30):7520-7536.
7. Monteiro M*, et al.* (2010) Identification of regulatory Foxp3+ invariant NKT cells induced by TGF-β. *J Immunol* 185(4):2157-2163.
8. Garcia ADR, Doan NB, Imura T, Bush TG, & Sofroniew MV (2004) GFAP-expressing progenitors are the principal source of constitutive neurogenesis in adult mouse forebrain. *Nature Neuroscience* 7(11):1233-1241.
9. Chen S, Lee B, Lee AYF, Modzelewski AJ, & He L (2016) Highly Efficient Mouse Genome Editing by CRISPR Ribonucleoprotein Electroporation of Zygotes. *J Biol Chem* 291(28):14457-14467.
10. Aton SJ*, et al.* (2013) Visual experience and subsequent sleep induce sequential plastic changes in putative inhibitory and excitatory cortical neurons. *Proc Natl Acad Sci U S A* 110(8):3101-3106.
11. Ognjanovski N, Maruyama D, Lashner N, Zochowski M, & Aton SJ (2014) CA1 hippocampal network activity changes during sleep-dependent memory consolidation. *Front Syst Neurosci* 8:61.

12. Hill DN, Mehta SB, & Kleinfeld D (2011) Quality metrics to accompany spike sorting of extracellular signals. *J Neurosci* 31(24):8699-8705.
13. Sato T, Suzuki T, & Mabuchi K (2007) Fast automatic template matching for spike sorting based on Davies-Bouldin validation indices. *Conf Proc IEEE Eng Med Biol Soc*:3200-3203.
14. Nicolelis MA*, et al.* (2003) Chronic, multisite, multielectrode recordings in macaque monkeys. *PNAS* 100(19):11041-11046.
15. Herry C*, et al.* (2008) Switching on and off fear by distinct neuronal circuits. *Nature* 454(7204):600-606.
16. Bortone DS, Olsen SR, & Scanziani M (2014) Translaminar inhibitory cells recruited by layer 6 corticothalamic neurons suppress visual cortex. *Neuron* 82(2):474-485.